



## Review

## Microfluidic impedance cytometry for single-cell sensing: Review on electrode configurations

Shu Zhu, Xiaozhe Zhang, Zheng Zhou, Yu Han, Nan Xiang<sup>\*</sup>, Zhonghua Ni<sup>\*\*</sup>

School of Mechanical Engineering, And Jiangsu Key Laboratory for Design and Manufacture of Micro-Nano Biomedical Instruments, Southeast University, Nanjing, 211189, China

## ARTICLE INFO

## Keywords:

Single-cell analysis  
Microfluidic impedance cytometry  
Electrode configurations  
Label-free

## ABSTRACT

Single-cell analysis has gained considerable attention for disease diagnosis, drug screening, and differentiation monitoring. Compared to the well-established flow cytometry, which uses fluorescent-labeled antibodies, microfluidic impedance cytometry (MIC) offers a simple, label-free, and noninvasive method for counting, classifying, and monitoring cells. Superior features including a small footprint, low reagent consumption, and ease of use have also been reported. The MIC device detects changes in the impedance signal caused by cells passing through the sensing/electric field zone, which can extract information regarding the size, shape, and dielectric properties of these cells. According to recent studies, electrode configuration has a remarkable effect on detection accuracy, sensitivity, and throughput. With the improvement in microfabrication technology, various electrode configurations have been reported for improving detection accuracy and throughput. However, the various electrode configurations of MIC devices have not been reviewed. In this review, the theoretical background of the impedance technique for single-cell analysis is introduced. Then, two-dimensional, three-dimensional, and liquid electrode configurations are discussed separately; their sensing mechanisms, fabrication processes, advantages, disadvantages, and applications are also described in detail. Finally, the current limitations and future perspectives of these electrode configurations are summarized. The main aim of this review is to offer a guide for researchers on the ongoing advancement in electrode configuration designs.

## 1. Introduction

Single-cell analysis has been emphasized to provide biologists and scientists with the opportunity to peer into the molecular machinery of individual cells and has been applied in chemistry [1], biology [2], food [3], medicine [4–6], and environmental monitoring fields [7]. Average and individual cell information through measurement of large populations of cells can provide early signals of disease or abnormal conditions in the human body. For example, tumor cells released into the bloodstream provide information on tumor development and treatment effectiveness [8]. The number of abnormal red blood cells (RBCs) in the blood can be used to diagnose diseases such as sickle cell anemia or polycythemia vera [9]. The cytoplasm conductivity and membrane permittivity of RBCs can be measured for diagnosing *Plasmodium* infection [10], and platelet cell counts are useful for monitoring and determining the risk of dengue shock syndrome [11].

Flow cytometry, as a well-established technique in the field of

biotechnology, has been widely used in single-cell analysis, owing to its high throughput (>1000 cells/s) and high sensitivity [12–14]. In conventional flow cytometry, cells labeled using fluorescent antibody pass through a focused beam of laser light, and the characteristic absorption, reflection, scattering, or fluorescence emission of the cells are identified for cell classification [15,16]. This method has been used in clinical medicine for purposes, such as enumerating lymphocyte subsets [17], identifying and purifying hematopoietic and other stem cells [18,19], analyzing cell survival rate [20], as well as detecting and identifying cancer types [21]. Nevertheless, the laborious cell preparation steps of fluorescent staining cause the loss of living cells for further biochemical analyses [22]. Moreover, conventional flow cytometry also requires a complex particle focusing system, as well as a costly and bulky optical equipment [23]. For instance, the weight of the Beckman Coulter FC-500 can reach 80 kg and the price is up to \$100,000.00 [24], which markedly limits its use for point-of-care (POC) applications.

Benefiting from the rapid advancement in microfabrication and

<sup>\*</sup> Corresponding author.<sup>\*\*</sup> Corresponding author.E-mail addresses: [nan.xiang@seu.edu.cn](mailto:nan.xiang@seu.edu.cn) (N. Xiang), [nzh2003@seu.edu.cn](mailto:nzh2003@seu.edu.cn) (Z. Ni).

microfluidic techniques, many lab-on-a-chip (LOC) devices fabricated with microscale electrodes and channels have emerged for impedance-based single-cell analysis in disease diagnosis [25], drug screening [26], and differentiation fields [27–29]. These devices, termed microfluidic impedance cytometry (MIC), were developed from Coulter counter, which is used as a standard apparatus for blood analysis, in 1956 [30]. Unlike the conventional flow cytometer, MIC devices offer the advantages of having a small footprint, less reagent consumption, ease of use, noninvasive, and label-free detection for POC testing [31, 32]. In MIC devices, the cells are first suspended in solution and injected into the microchannel. Upon reaching the sensing zone composed of microelectrodes, the cells are individually interrogated by the electric field applied through the microelectrodes [33]. For each cell, the cytometry system collects the sensing impedance signals. These signals can extract information regarding the size, shape, and dielectric properties of the cells based on the Maxwell mixture theory [34]. However, the detection sensitivity and reliability of the current MIC devices are far from those of the conventional flow cytometer [35,36]. According to recent studies, electrode configuration plays an important role in improving detection sensitivity and reliability [37–39]. The electrode configuration can be classified into three main categories: two-dimensional [40–42], three-dimensional [20,43], and liquid electrode configurations [44,45]. The two-dimensional electrode configuration usually arranges electrodes on one side of the channel; it has the advantages of simple structure and fabrication and ease-of-integration. However, this configuration also causes nonuniformity of the applied electric field in the sensing zone, resulting in detection errors [37]. Compared to a two-dimensional electrode configuration, a three-dimensional electrode configuration typically sets multiple electrodes on the facing sides of the channel. This arrangement makes the applied electric field more uniform, and it is more suitable for high accuracy and sensitivity sensing [46]. Nevertheless, this configuration requires complicated and time-consuming fabrication processes (such as precise alignment), limiting its comprehensive applications for POC testing [47]. The liquid electrode configuration is an essential part of MIC devices [48], and it is set up using a conductive liquid. This configuration usually has a simple structure but is characterized by poor sensitivity owing to the fluctuation of the conductive liquid when flowing.

As a rapidly expanding technique, MIC has drawn much attention from researchers. Several reviews have been published in well-known journals [49–51], but they typically focus on fabrication methods and biomedical and clinical applications of state-of-the-art MIC devices. Electrode configuration in MIC devices plays a vital role in cell sensing; however, to the best of our knowledge, this aspect has not yet been reviewed. In this review, we present a panoramic view of the various electrode configurations, with emphasis on the influence of electrode shape and arrangement on cell sensing. The review begins with a brief discussion of the theoretical background of the impedance technique for single-cell analysis. Then, it highlights the two-dimensional, three-dimensional, and liquid electrode configurations (Fig. 1A). The sensing mechanisms, fabrication processes, advantages/disadvantages, and applications of these devices are also discussed in detail. Finally, the current limitations and future developments of these electrode configurations are summarized. The main objective of this review is to offer a guide for the development of novel electrode configurations and thereby improve the sensing accuracy and throughput of MIC devices.

## 2. Theory

### 2.1. Cell modeling

Electrical impedance is the ratio of the excitation voltage to the response current when a cell passes through the sensing zone.

$$\tilde{Z} = \frac{\tilde{V}}{\tilde{I}} \quad (1)$$

where  $\tilde{Z}$  is the electrical impedance,  $\tilde{V}$  is the applied voltage, and  $\tilde{I}$  is the response current.

The response current reflects the dielectric properties of target cells and host medium [52,53]. As a particle or cell passes through the sensing zone, it causes an electric field change owing to the differences in permittivity or conductivity between the cells and the medium. Cells cannot be regarded as homogenous, and different components of cells, such as membrane and cytoplasm, should be modeled for estimating the complex permittivity of cells [54,55]. The single-shelled spherical model (Fig. 1B), which is composed of a conducting sphere (cytoplasm) and an insulating thin shell (cell membrane), has been widely used to analyze

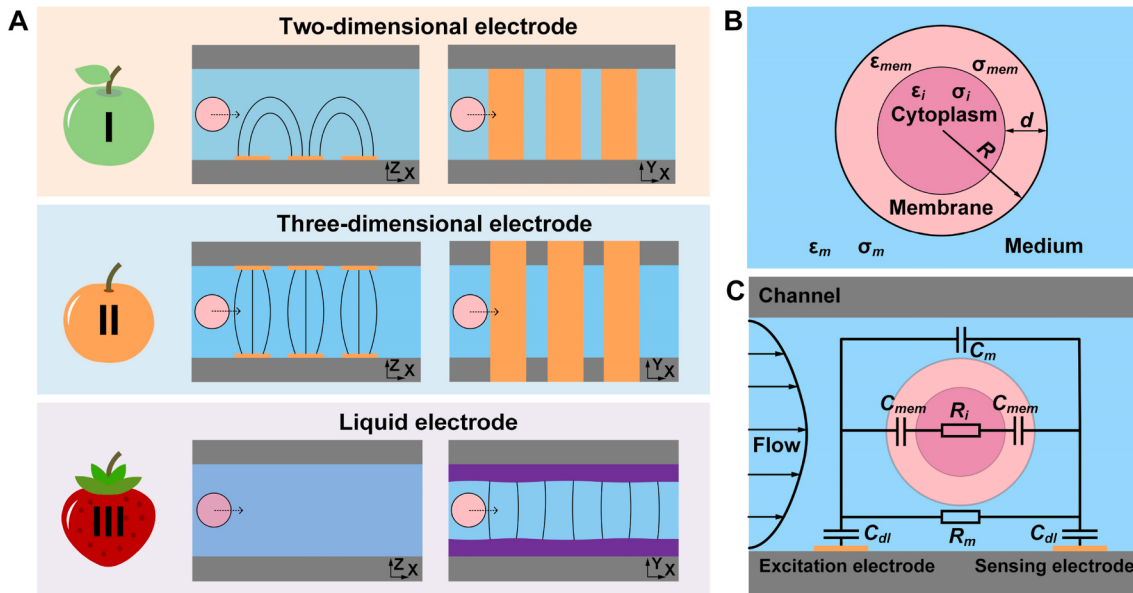


**Fig. 1.** (A) Electrode configurations in microfluidic impedance cytometry. (B) Single-shell model for a single cell in suspension,  $\epsilon_m$ ,  $\epsilon_{mem}$  and  $\epsilon_i$  refer to the complex permittivities of the suspending medium, cell membrane, and cytoplasm;  $\sigma_m$ ,  $\sigma_{mem}$ , and  $\sigma_i$  represent the conductivity of the medium, cell membrane, and cytoplasm. (C) Equivalent circuit model for a single cell between two electrodes.

the obtained results of impedance measurements [56,57]. Therefore, the complex permittivity of the cell  $\tilde{\epsilon}_p$  can be calculated as follows:

$$\tilde{\epsilon}_p = \tilde{\epsilon}_{mem} - \frac{\gamma^3 + 2 \left( \frac{\tilde{\epsilon}_i - \tilde{\epsilon}_{mem}}{\tilde{\epsilon}_i + 2\tilde{\epsilon}_{mem}} \right)}{\gamma^3 - \left( \frac{\tilde{\epsilon}_i - \tilde{\epsilon}_{mem}}{\tilde{\epsilon}_i + 2\tilde{\epsilon}_{mem}} \right)} \quad (2)$$

where  $\tilde{\epsilon}_{mem}$  and  $\tilde{\epsilon}_i$  refer to the complex permittivities of the cell membrane and cytoplasm, respectively;  $\gamma = (R + d)/R$ , where  $R$  and  $d$  represent the inner radius and membrane thickness of the cell, respectively.

For the suspension of cell/particle, the complex permittivity is generally simulated using Maxwell's mixture theory. The complex permittivity for the medium-cell mixture  $\tilde{\epsilon}_{mix}$  is

$$\tilde{\epsilon}_{mix} = \tilde{\epsilon}_m \frac{1 + 2\Phi\tilde{f}_{CM}}{1 - \Phi\tilde{f}_{CM}} \quad (3)$$

where  $\tilde{\epsilon}_m$  represents the complex permittivity of the suspending medium,  $\Phi$  is the volume fraction of the cell/particle to the sensing zone, and  $\tilde{f}_{CM} = (\tilde{\epsilon}_p - \tilde{\epsilon}_m)/(\tilde{\epsilon}_p + 2\tilde{\epsilon}_m)$  is the Clausius-Mossotti factor.

For the cell-medium mixture, the complex impedance  $Z_{mix}$  is linked to its complex permittivity  $\tilde{\epsilon}_{mix}$  and can be calculated as

$$\tilde{Z}_{mix} = \frac{1}{j\omega\tilde{\epsilon}_{mix}G_f} \quad (4)$$

where  $j = \sqrt{-1}$ ,  $\omega$  is the electric field frequency, and  $G_f$  is a geometric constant that depends on the geometry of the detection zone. For single-cell impedance analysis, the value of  $G_f$  is the ratio of the electrode area to the gap for an ideal parallel-plate electrode system. However, the electric field generated by microelectrodes is usually not uniform, and the issue of the divergent field should be corrected [50].

According to equations (1)–(4), the dielectric properties of the particle/cell can be derived by measuring the complex impedance of the particle/cell suspension.

## 2.2. Equivalent circuit modeling

Impedance signals reflecting the information of cells can be acquired when a single cell passes through the electrode sensing zone. When a direct current (DC) voltage is applied to the electrodes, the cell/particle can be considered a homogenous insulating spherical particle, and the signal strength is relative to the ratio of the cell volume to the channel dimension [58]. When the applied signal is an alternating current (AC) voltage, the single-shelled spherical cell model is used to model the cell and acquire detailed information regarding the cell itself [59,60]. In 1989, Foster and Schwan proposed a simplified equivalent circuit model for simplifying the analysis of the system [61]. Generally, the resistance of the cell membrane is much larger than its capacitance and can be ignored; the capacitance of the cytoplasm can also be ignored because the capacitance is much smaller than its resistance. Therefore, as shown in Fig. 1C, the cell is approximated to a resistor that represents the cytoplasm ( $R_i$ ) in series with two capacitors that describe the membrane ( $C_{mem}$ ). In addition, the impedance is dependent on the medium resistance ( $R_m$ ), medium capacitance ( $C_m$ ), and electrical double-layer capacitance ( $C_{dl}$ ). Electrical double-layer capacitance appears at the interface between the surface of the electrode and an adjacent liquid electrolyte [62]. Typically,  $C_{dl}$  increases with the surface area of the electrode. According to the equivalent circuit model, large  $C_{dl}$  and  $R_m$  can result in the attenuation of the measured particle and cell signals. Therefore, electrode with small electrical double-layer capacitance and liquid media with high conductivity are beneficial to high sensitivity cell sensing. Specifically, the values of other electrical components are

described as follows:

$$R_m = \frac{1}{\sigma_m(1 - 3\Phi/2)G_f} \quad (5)$$

$$C_m = \epsilon_\infty G_f \quad (6)$$

$$C_{mem} = \frac{9\Phi RC_{mem,0}}{4} G_f \quad (7)$$

$$R_i = \frac{4(1/2\sigma_m + 1/\sigma_i)}{9\Phi G_f} \quad (8)$$

where  $C_{mem,0} = \epsilon_{mem}/d$  represents the specific membrane capacitance (per unit area),  $\epsilon_\infty \cong \epsilon_m[1 - 3\Phi(\epsilon_m - \epsilon_i)/(2\epsilon_m + \epsilon_i)]$  represents the high-frequency permittivity at limit, and  $\sigma_m$  and  $\sigma_i$  represent the conductivity of the medium and cytoplasm, respectively.

In the equivalent circuit modeling, as the cell membrane and electrical double-layer are treated as capacitors, thus the  $C_{mem}$  and  $C_{dl}$  will change with the applied AC frequency ( $\omega$ ). In the low-frequency range ( $\omega < 1$  MHz), the electrical double layer dominates the system impedance; thus, the sensitivity for detecting a single cell is very low. As the frequency increases (1 MHz  $< \omega <$  100 MHz), the electrical double-layer capacitance gradually decreases, and the system impedance is dominated by the cell size. At a higher frequency range ( $\omega > 100$  MHz), the system impedance mainly depends on the cytoplasm resistance, because the membrane capacitance is short-circuited in this frequency range. Foster and Schwan's equivalent circuit model provided good agreement with experiments for calculating single-cell impedance. However, cell membrane conductance and cytoplasm capacitance should also be considered in certain cases, such as electroporation and cell lysis. Under these circumstances, a complete equivalent circuit model that contains membrane resistance and cytoplasm capacitance is required. Sun et al. discussed the full details for calculating the values of  $R_i$ ,  $C_i$ ,  $R_{mem}$ , and  $C_{mem}$  [49,63].

Before cell sensing, researchers usually sweep the MIC device in a certain frequency range to ensure no significant changes over the device impedance. Additionally, many researchers also calibrate the impedance signals of individual cells using standard polystyrene beads during each measurement.

## 3. Two-dimensional electrode

### 3.1. Two-electrode configuration

In a two-dimensional two-electrode configuration, electrodes are usually laid on the bottom or top of the channel. An AC voltage is applied through the electrodes, forming a sensing zone. As cells flow through this zone, the electric field between two electrodes is disrupted, causing a current change that can extract information regarding the dielectric properties of cells [64]. Based on this mechanism, Lin et al. developed an MIC device that sets a pair of Au electrodes on the bottom of the microchannel to detect proteins on the surfaces of cancer cells (Fig. 2A) [65]. The AC voltage was applied to one of the electrodes, and the other was used to receive the impedance response signal. Bare magnetic beads, cancer cells, and bead-cell aggregates can be differentiated according to their impedance and frequency responses. This device could also be applied to detect and assess the surface membrane-bound protein (e.g., matriptase) levels, as the impedance amplitude of bead-cell aggregates is proportional to the concentration of matriptase expressed on the cancer cells. The Au electrode has the advantages of electrochemical corrosion resistance but is expensive and difficult to fabricate. The conventional Au electrode fabrication method requires steps, including standard photolithography [66]. To simplify the manufacturing processes and turn the MIC device into a disposable device, researchers have proposed many methods. For example, researchers fabricated electrodes by depositing Cu on a commercially available printed circuit

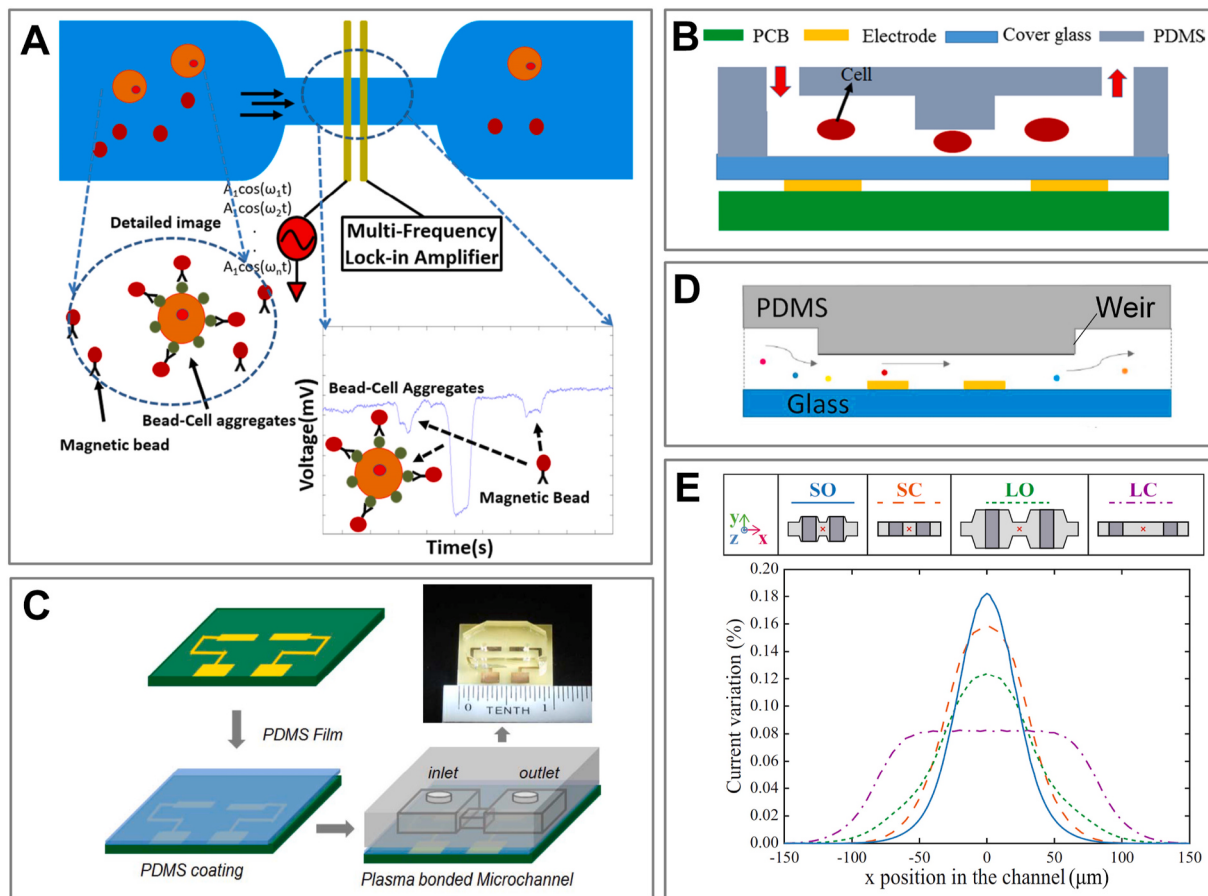


**Fig. 2.** (A) Two Au electrodes for detecting proteins on surfaces of cancer cells. Reprinted with permission from Ref. [65]. Copyright 2020, Springer Nature. (B) Electrodes fabricated by depositing Cu on PCB. Reprinted with permission from Ref. [24]. Copyright 2017, Springer Nature. (C) Cu electrodes coated with thin PDMS film. Reprinted with permission from Ref. [67]. Copyright 2016, Institute of Electrical and Electronics Engineers. (D) Weir structure above electrodes. Reprinted with permission from Ref. [68]. Copyright 2020, Elsevier. (E) The optimized channel and electrode structure for high sensing sensitivity. Reprinted with permission from Ref. [69]. Copyright 2019, Springer Nature.

board (PCB) [24]. Then a microchannel with a glass cover was laid on the PCB (Fig. 2B). The AC voltage applied to the electrodes can penetrate the glass cover for cell sensing. In their device, WBCs and circulating tumor cells (CTCs) were successfully differentiated from a mixture of RBCs, WBCs, and CTCs. In addition, Ren et al. used the same technique to manufacture the electrodes, but isolated the electrodes from the channel using a thin PDMS film to protect the Cu electrodes from electrochemical reactions (Fig. 2C) [67]. In this device, the response signals of the HeLa cells could be obtained. In the two-electrode configuration, electrodes were placed on one side of the channel, causing a non-homogenous electric field along the vertical direction of the channel. To alleviate the interference of this phenomenon, researchers set a weir above the electrode zone (Fig. 2D), which can ensure that the cell passes through the center-line of this zone as far as possible [68]. Besides, channel structures around the electrode zone and the distance between the two electrodes can also affect sensing signals. Cottet et al. presented a comprehensive study for enhancing the electrical impedance sensitivity by optimizing the channel and electrode structure (Fig. 2E) [69]. It was found that a smaller distance between the two electrodes provided a high sensing sensitivity on the centered particles.

Cell shape as a fundamental biological feature offers much information regarding cellular physiological and pathological conditions and thus can be used to distinguish different types of cells [70]. To achieve this purpose, a constricted channel was embedded in a two-electrode configuration [71]. Specifically, for spherical or rod-shaped cells, the constriction zone in the channel could focus the particle stream, align the particle axis with the streamline, and form single-cell flow as the cell

passes through the sensing zone (Fig. 3A). The rod cells experienced a longer passing time than the spherical cells did, resulting in different widths, amplitudes, and the ratio of width to amplitude of the impedance signals. Using this technique, typical late-budding, early-budding, and unbudded yeast cells were classified by calculating the amplitude and width of the impedance signal, whereas the late-budding rate, which can serve as an index of the reproductive rate, was successfully estimated using the amplitude and ratio of width to amplitude. Furthermore, microorganisms with variable morphologies can also be identified using these techniques. For instance, Zhu et al. used a similar structure to measure *Caenorhabditis elegans* (*C. elegans*) worms (Fig. 3B) [72]. Since worm length represents the development of *C. elegans*, their developmental stages could be obtained after analyzing the amplitude and width of the measured signals.

In addition to the aforementioned impedance cytometry, the shape and arrangement of the conventional two-electrode configuration can be revised to achieve special purposes. For instance, to enhance the sensitivity of cell position estimation, Brazey et al. designed a pair of star-shaped electrodes in their device [73]. The relative position error between the cell and the electrode may induce inaccurate cell sensing. The classical two-electrode configuration is not suitable for cell position sensing because the response signal at the area between the two electrodes was constant (Fig. 4A). In contrast, the response signal using the star-shaped electrodes is variable, which can acquire the position information of cells after analyzing the signal geometry. This study also used an extended Kalman filter to estimate the cell position despite drift and signal noise and achieved real-time detection. In addition, Wang

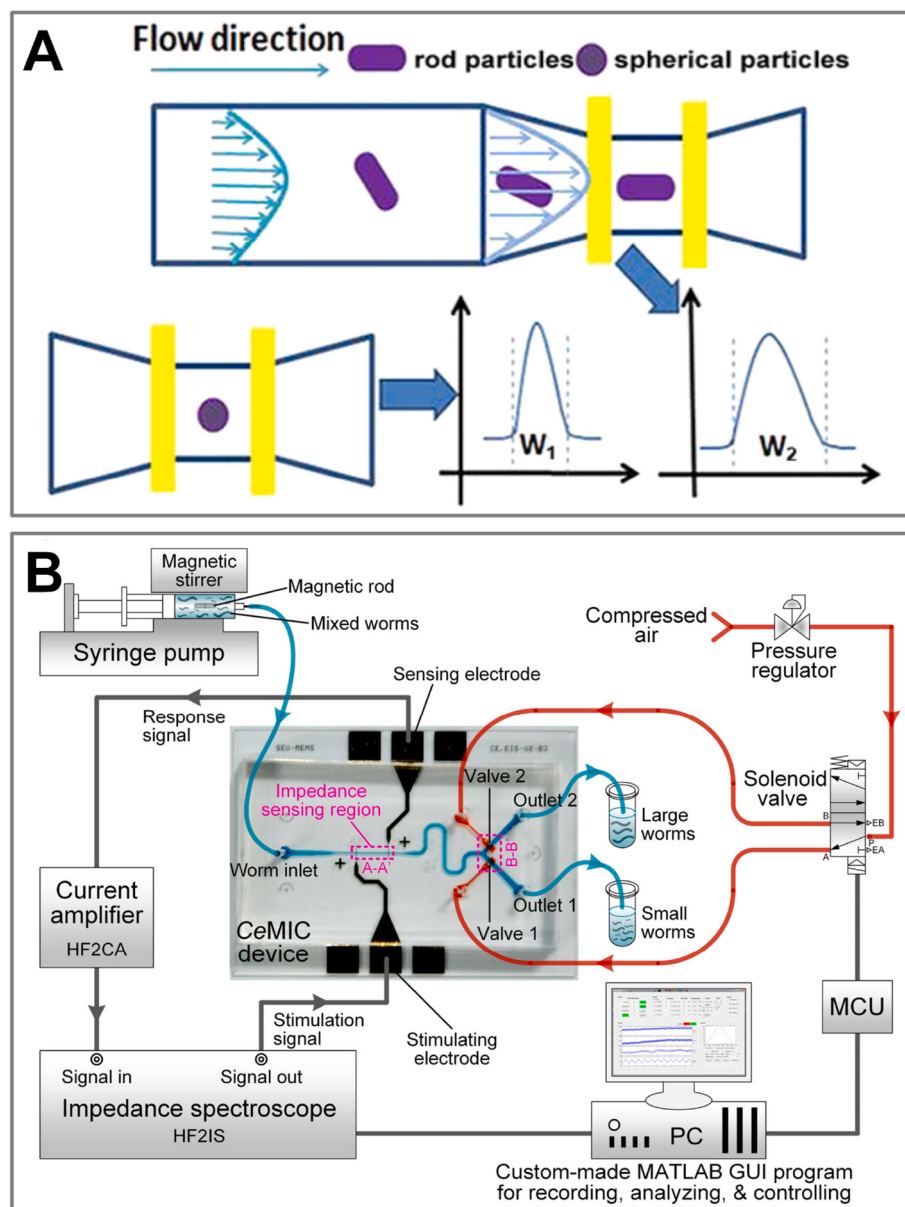


**Fig. 3.** (A) Constriction zone in two electrodes for aligning rod particle axis with streamline. Reprinted with permission from Ref. [71]. Copyright 2019, American Chemical Society. (B) Constriction zone in two electrodes for detecting *C. elegans* worms. Reprinted with permission from Ref. [72]. Copyright 2018, Elsevier.

et al. presented a cell-position detection technology using a pair of nonparallel electrodes [74]. In contrast to traditional parallel electrodes, impedance signals with different amplitudes and widths can be generated when the cell flows through the electrode zone at different transverse positions. Thus, as illustrated in Fig. 4B, the transverse position of the cells can be determined by evaluating the impedance signals. In their device, the transverse positions of cells/particles, which have diameters ranging from 6 to 11  $\mu\text{m}$ , can be differentiated clearly. Researchers have also modified the two-electrode configuration by adding another electrode. For example, Zi et al. developed an MIC device composed of a pair of two-electrode configurations and a mixing zone to investigate the cell survival rate (Fig. 4C) [75]. The first electrode zone was used for cell counting, and then the cells flowed into the mixing zone to achieve rapid mixing of the cell suspension and hypertonic solution. The hypertonic stimulus could enhance the volume difference between live and dead cells because dead cells lose osmoregulatory function and membrane integrity and remain unchanged, whereas the living cells shrink. Therefore, the second electrode zone was used to recount the cells and

determine the volume of cells after exposure to the hypertonic solution. According to the conventional volume distributions of living and dead human umbilical vein endothelial cells (HUEVCs), human colon cancer (HT-29) cells, and immature bone marrow-derived macrophage (iBMDM) cells, the corresponding percentages of living or dead cells could be calculated by analyzing the cell shrinkage rate. In addition, by designing the microfluidic channel reasonably, a pair of the two-electrode configurations placed at the bottom of the channel could achieve the impedance sensing for flowing cells and trapped cells simultaneously [76]. From Fig. 4D, the microfluidic channel contains an array of cell pass-and-stay units; each unit has a main channel bifurcating to the bypassing path that allows the cell to flow through, and a trapping path that allows the cell to be trapped in a narrow constriction. The first two-electrodes placed underneath the main channel could obtain discrete impedance data points of the flowing cells, while the second two-electrode set in the narrow constriction was able to acquire the impedance spectrum of the trapped cell. Flowing cell measurement revealed the impedance magnitude differences of a large number of

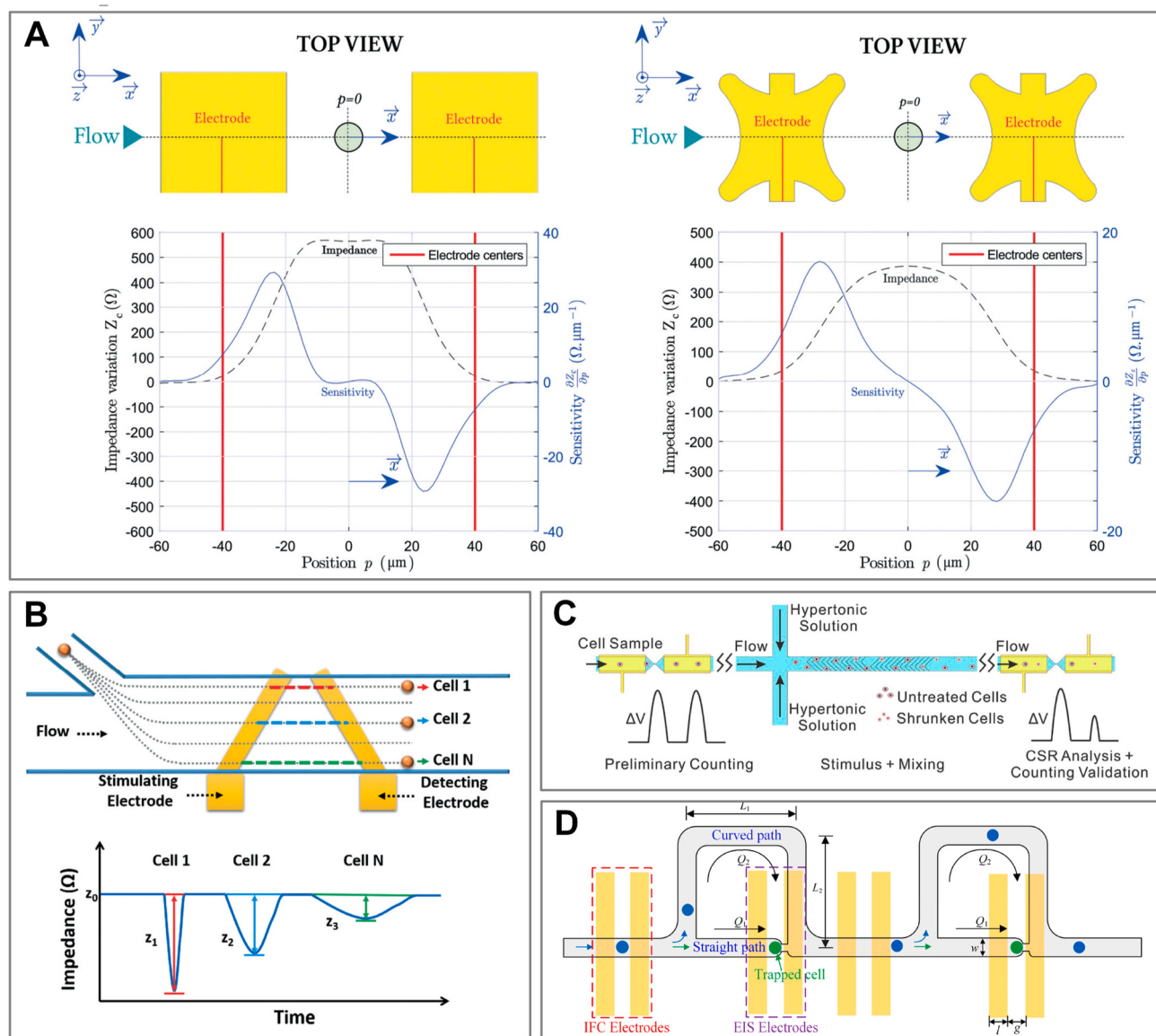


**Fig. 4.** (A) Star-shaped electrodes for estimating cell position. Reprinted with permission from Ref. [73]. Copyright 2018, Royal Society of Chemistry. (B) The two nonparallel electrodes for detecting the transverse position of the cell. Reprinted with permission from Ref. [74]. Copyright 2017, Royal Society of Chemistry. (C) Two-electrode configuration embedded with a mixing zone. Reprinted with permission from Ref. [75]. Copyright 2020, Elsevier. (D) Two two-electrode configurations placed underneath the channel for detecting flowing and trapped cells separately. Reprinted with permission from Ref. [76]. Copyright 2019, American Chemical Society.

cells, while trapped cell measurement enabled quantification of area-specific membrane capacitance and cytoplasmic conductivity. Cancer cells, including HeLa, A549, and HepG2, were found to have significant differences in sensing signal magnitude, cytoplasmic conductivity, and specific membrane capacitance.

The two-electrode configuration has the advantages of simple structure and easy fabrication, and it has been extensively researched for wider applications. For instance, acquiring inherent cell information and tracking the cell trajectory. However, this configuration usually suffers from high background noise and uneven drift of the electrode properties, thereby decreasing the sensing sensitivity. Increasing the excitation voltage can lead to a high signal-to-noise ratio (SNR), but may cause electrochemical reactions, form bubbles, and induce cell membrane damage.

### 3.2. Three-electrode configuration

To increase the sensing sensitivity, Gawad and colleagues first proposed a three-electrode configuration in their MIC device for differentially measuring impedance signals [77]. The central electrode was applied with AC voltage (Fig. 5A), and the lateral two electrodes received electric currents with opposite phases. When a cell passes through the first half of the sensing zone, the electric current fluctuation can be measured; the second half measures the electric current passing through the medium, which acts as a reference. Moreover, the measurement was realized by sensing the differential variations of these two impedance signals. Because the measurement and reference electrodes were inherently switched, the differential variation in impedance acted as a pair of peaks. Typically, the electric current captured from two lateral electrodes can be transferred into voltage signals using trans-impedance amplifiers. The differential variation between the two signals was achieved using a differential amplifier. In addition, the lock-in

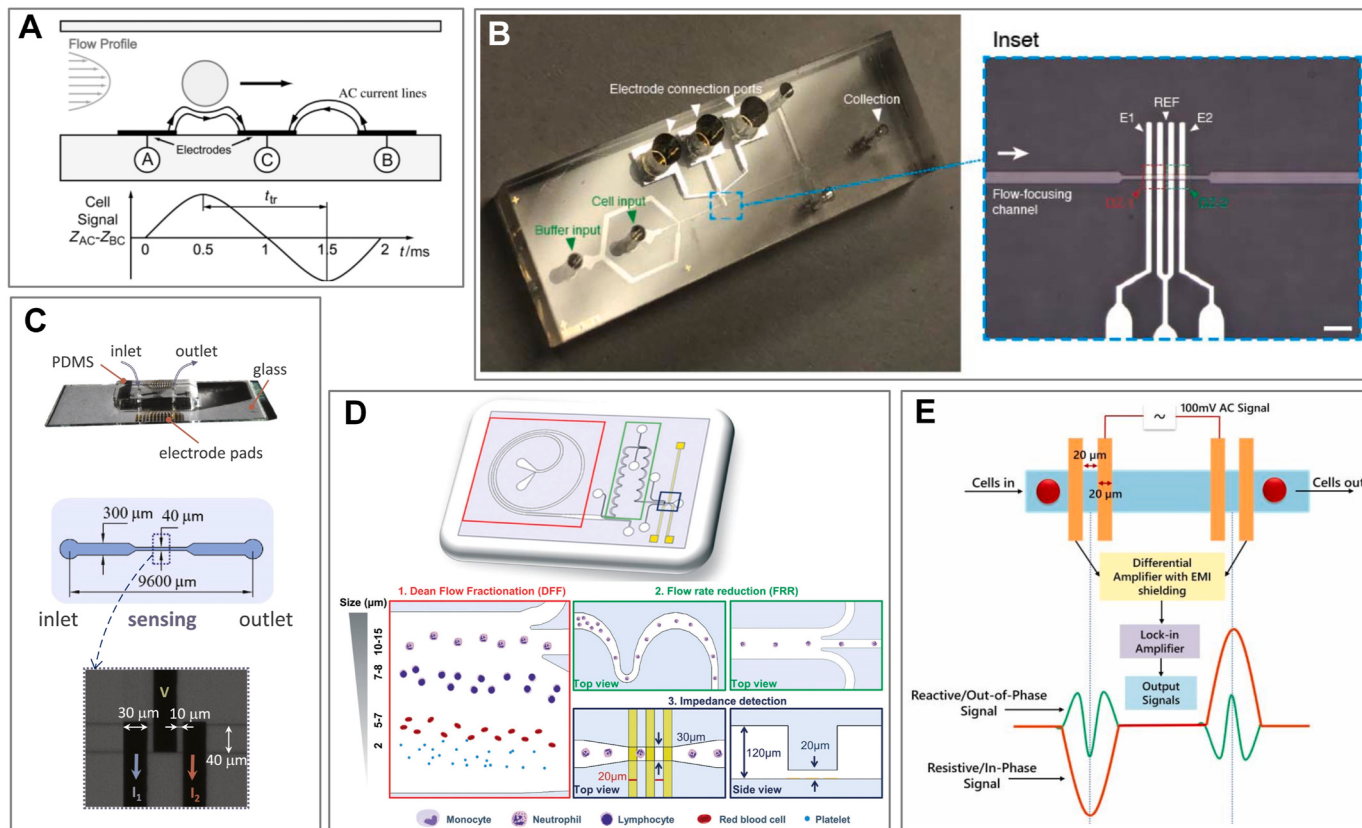


**Fig. 5.** (A) Three-electrode configuration for differential measurement. Reprinted with permission from Ref. [77]. Copyright 2001, Royal Society of Chemistry. (B–C) Applications of three-electrode configuration. (B) Reprinted with permission from Ref. [78]. Copyright 2019, Institute of Electrical and Electronics Engineers. (C) Reprinted with permission from Ref. [79]. Copyright 2020, Elsevier. (D) The three-electrode configuration coupled with an inertial spiral channel and serpentine channel. Reprinted with permission from Ref. [81]. Copyright 2019, Royal Society of Chemistry. (E) The “double peak behavior” when the cell is passing through. Reprinted with permission from Ref. [84]. Copyright 2020, Royal Society of Chemistry.

amplifier was able to demodulate the in-phase and out-of-phase current signals at excitation frequencies while rejecting noise at other frequencies. Using this device, erythrocytes and ghost cells were discriminated by analyzing their signal in-phase amplitudes recorded at two frequencies. This differential impedance sensing scheme can correct any uneven drift in the properties of the electrodes and increase the sensing sensitivity. As a result, it is the most common structure for single-cell impedance sensing. Based on this configuration, Desai et al. successfully differentiated dissociated tumor cells from RBCs and peripheral blood mononuclear cells according to the differences in their response signal magnitudes (Fig. 5B) [78]. In addition, De Dinno et al. characterized viable, necrotic, and apoptotic human lymphoma U937 cells using the differences in signal magnitude and phase at multiple frequencies (Fig. 5C) [79]. Apoptotic, necrotic, and viable cells were characterized by different sizes and dielectric properties, which caused different impedance signatures for these cells. Moreover, in their device, they proved that signal magnitude at low frequency allows the classification between viable/necrotic cells and apoptotic bodies, whereas the signal phase enables the differentiation between viable cells and necrotic cells. Petchakup et al. used the three-electrode configuration for identifying different leukocyte subtypes, investigating leukocyte activation, monitoring monocyte differentiation, and characterizing monocyte subtypes [80]. In contrast to other research groups, for whom isolation of leukocytes from the blood relied on expensive and time-consuming affinity-based antibody binding steps, this group obtained leukocytes using the cost-effective Dean Flow Fractionation technology. Later, the same group coupled spiral inertial microfluidics with a three-electrode impedance cytometer, constructing an integrated platform for continuous and label-free leukocyte sorting and impedance

sensing (Fig. 5D) [81]. In diabetes testing, they observed significant differences between the formation of neutrophil extracellular traps (NETosis) by healthy and glucose-treated neutrophils, as well as between calcium ionophore- and phorbol 12-myristate 13-acetate-induced NETosis profiles, according to the impedance response magnitude and electric opacity (the ratio of impedance response magnitude at high frequency to that at low frequency) of cells. More recently, this group combined this integrated platform with a magnetic activated cell sorting method for impedance profiling of CD4<sup>+</sup> T-lymphocytes response in peripheral blood mononuclear cells stimulated with Tuberculin Purified Protein Derivative (PDD) antigen [82]. Their platform showed better sensitivity than immunophenotyping by conventional flow cytometry. The measured impedance for low-conductivity liquids, such as samples containing pathogenic bacteria or microalgae, can increase by up to 30-folds compared to that for physiological liquids. Moreover, at high frequencies, the parasitic coupling capacitance of the sensor can short circuit the sample impedance. Claudel et al. developed a complete electric model of the three-electrode configuration to optimize the sensor under low-conductivity liquids [83]. Their research results proved that the electrode and track placement should be taken into consideration in the case of low-conductivity liquid analysis. They successfully characterized the impedance properties of yeast cells in low-conductivity liquids using an optimized electrode configuration, which is difficult to accomplish using conventional electrodes. When the cell passed through the three-electrode configuration, Mahesh et al. observed an unusual “double peak behavior” featured in the phase of the response signal at an excitation frequency of 400–800 kHz (Fig. 5E) [84]. At a relatively low frequency, the impedance response is mainly caused by the cell membrane capacitance, and the reactive current

passing through the cell is smaller than that passing through its surrounding medium. When the cell moves above the sensing electrode, a larger current density can generate a momentary increase in the reactive current and induce a response signal phase increase. As the cell moves between the exciting and sensing electrodes, the presence of the cell reduces the cross-section of the channel, resulting in a decrease in the reactive current and response signal phase. Therefore, “double peak behavior” can be observed. Since the “double peak behavior” is related to the cell membrane capacitance, normal and glutaraldehyde-treated RBCs could be differentiated accurately by analyzing these double peak profiles. Compared to conventional multi-frequency cell sensing, this technique can acquire information on both cell size and membrane capacitance at a single frequency.

These planar electrodes placed at the top or bottom of the channel usually cause a nonhomogeneous electric field, resulting in the variation in the impedance signal with the cell position in the sensing zone [50]. Therefore, bioparticles with large sizes (such as 3D cellular spheroids/microcarriers, with diameters of 100  $\mu\text{m}$ -1 mm) were more suitable for these impedance sensing configurations [85]. When detecting bioparticles with small size ( $<20 \mu\text{m}$ ), positional dependence of the impedance sensing signal is a challenge for high-sensitivity detection of MIC devices. To overcome this limitation, numerous particle-focusing techniques have been integrated into the three-electrode impedance cytometry. For instance, the weir structure above the electrode zone mentioned in the two-electrode configuration was also used here [81]. In addition, the viscoelastic focusing technique can ensure particles focus in a single train [86]. Based on this technique, Serhatlioglu et al. developed an MIC device that integrated viscoelastic focusing and impedance sensing units (Fig. 6A) [87]. The RBCs could be aligned along the channel centerline when passing through the sensing zone, yielding consistent and stable impedance signals. In their study, single stable signals for polystyrene beads and RBCs were obtained. Another method to address this limitation is to compensate for the signal variations caused by different particle flow trajectories. By modifying the three-electrode configuration, De Ninno et al. presented a novel five-electrode configuration for accurate particle sizing [88], even if the particle flows in different trajectories (Fig. 6B). Because the electric field strength gradually decreases away from the electrodes, identical particles flowing close to the electrodes or apart from the electrodes can yield high or low amplitudes, respectively. In such an impedance sensor, the differential signal exhibits a bipolar Gaussian profile. The relative prominence of the peaks with respect to the saddle between them could deduce the information regarding particle velocity and height, which can be used to correct the measured electrical diameter. Using this method, the authors acquired an excellent coefficient of variation in measuring polystyrene bead size and clearly differentiated yeast from polystyrene beads of similar size, as well as two yeast populations, which could not be realized without correction.

In practical applications, the MIC device usually needs to handle particle suspensions with high concentrations. However, two or more particles passing through the sensing zone nearly simultaneously may result in errors when measuring the properties of these particles. To address this problem, Caselli et al. reported a method using a Bayesian approach, enabling the decomposition of coinciding particle signals into individual particle contributions [89]. As shown in Fig. 7A, two pairs of three-electrode configurations were set at the bottom of the channel and separated by a hyperbolic constriction. Cells passing through the constriction part of the channel have higher velocity and different relative positions compared to those in the wider part of the channel, and thus generate two different signal shapes in the two sensing zones. By exploiting a Bayesian approach that uses a maximum a posteriori probability (MAP) estimation, the two different signal shapes of coinciding particles can be decomposed into single-particle components. Their experimental results demonstrated that this device can offer an accurate and fast characterization of cell suspensions with a concentration of  $5 \times 10^6 \text{ cells/mL}$ , which is far beyond similar MIC devices [90,

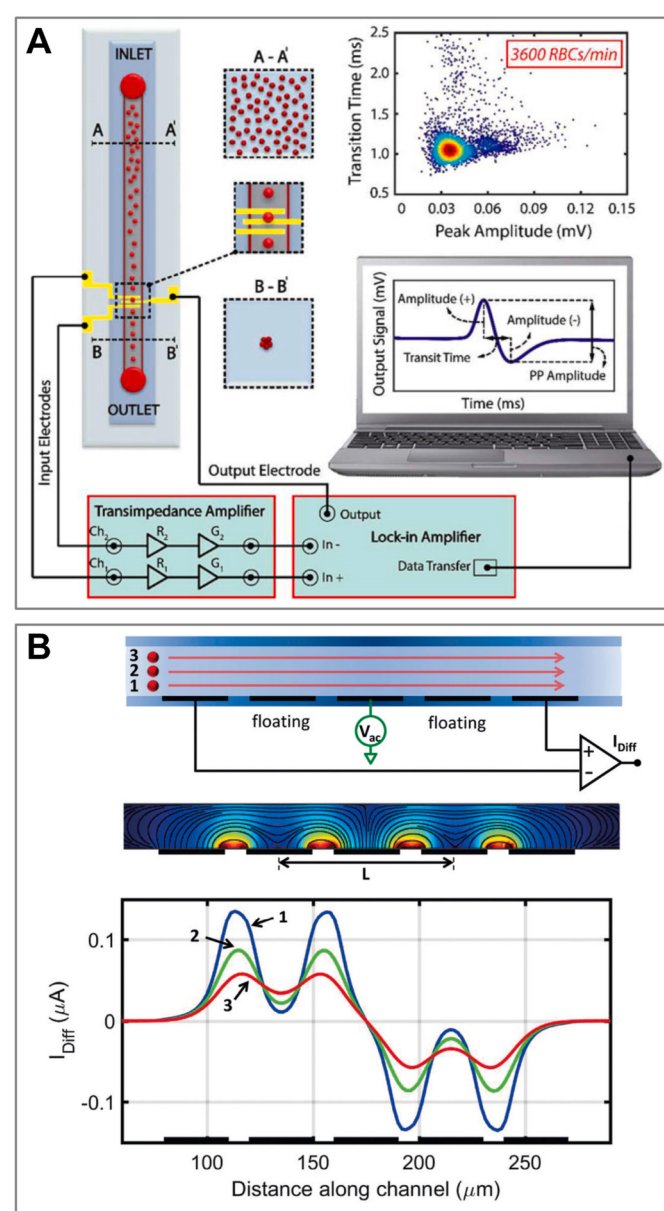


**Fig. 6.** (A) The MIC device integrated viscoelastic focusing with three-electrode units. Reprinted with permission from Ref. [87]. Copyright 2019, Wiley. (B) The five-electrode configuration, and signal profiles for particle flowing in different trajectories. Reprinted with permission from Ref. [88]. Copyright 2017, Royal Society of Chemistry.

[91]. In fact, tracking the lateral position of single cells in a microfluidic channel plays an important role in cell separation at high concentrations. To measure the lateral position of a single cell or particle in a continuous flow, researchers tilted the middle exciting electrode of the three-electrode system (Fig. 7B). If the cell passes through the lateral position close to the channel wall, the acquired differential signal exhibits a pair of asymmetric peaks owing to the slant electrode. The peak amplitude and width at both sides of the signal vary according to the lateral position of the cell. This device, presented by Yang et al., was able to determine the lateral position of RBCs in the channel with a deviation of 10.3  $\mu\text{m}$  and could characterize their physical properties simultaneously [92].

In many cases, the parameters of the response signal (such as amplitude, phase, and electric opacity) are insufficient for cell classification [59,93]. Therefore, apart from impedance sensing, researchers have introduced parameters related to cell mechanical properties to

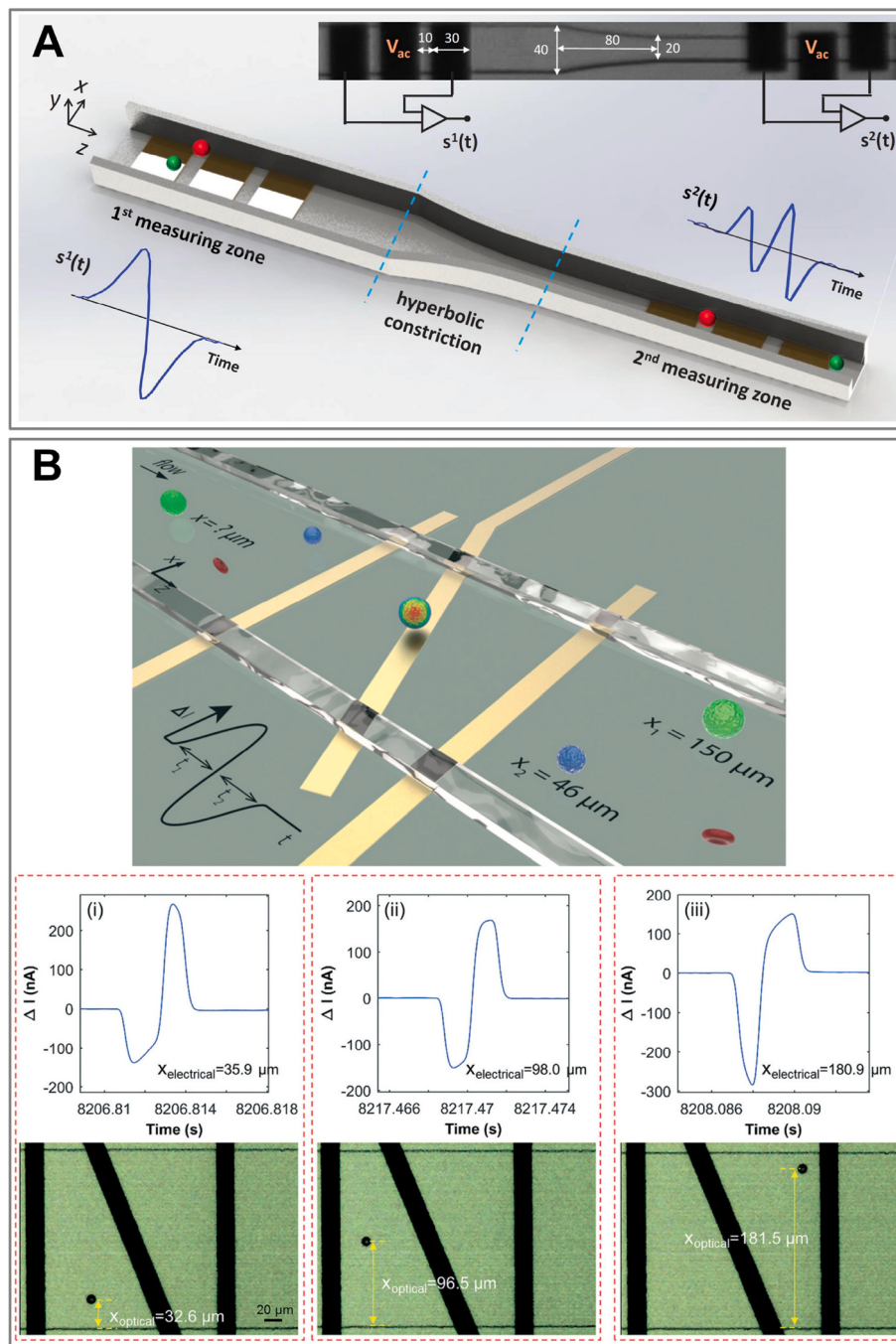


**Fig. 7.** (A) Two three-electrode configurations separated by a hyperbolic constriction. Reprinted with permission from Ref. [89]. Copyright 2020, Institute of Electrical and Electronics Engineers. (B) Three-electrode configuration with titled middle electrode for measuring lateral positions of particles. Reprinted with permission from Ref. [92]. Copyright 2019, Royal Society of Chemistry.

accurately identify cell populations. Han et al. proposed an MIC device embedded in a three-electrode system with a constriction channel to characterize the mechanical and electrical properties of single plant cells simultaneously (Fig. 8A) [94]. Cells with different deformabilities experience different passing times when they flow through the constriction channel. Because the constriction channel is embedded in the two pairs of electrodes, the cell differential current response and its corresponding passing time can be recorded simultaneously. Using this device, live protoplasts derived from *Arabidopsis* and *Populus*, as well as cells at various primary cell wall regeneration statuses, could be well differentiated according to their mechanical and electrical changes. Based on this principle, Zhou et al. developed a similar device but added

more electrodes to measure the total passage time, entry time, and transit time of cells in the constriction channel (Fig. 8B) [95]. By comprehensively evaluating the mechanical and electrical impedance properties, the cell populations of RBCs, MCF-7, PMA-modified MCF-7, and fixed MCF-7 cells were differentiated.

As one of the most widely used schemes, the three-electrode configuration is fabricated easily and offers a relatively high SNR for cell sensing, but the issue of electric field nonuniformity remains unresolved. Decreasing the cross-sectional area of the channel or sensing zone has been proposed, but it may cause clogging and reduce the sensing throughput. In addition, signal compensation strategies based on the electrical metrics of the particle position can increase the sensing

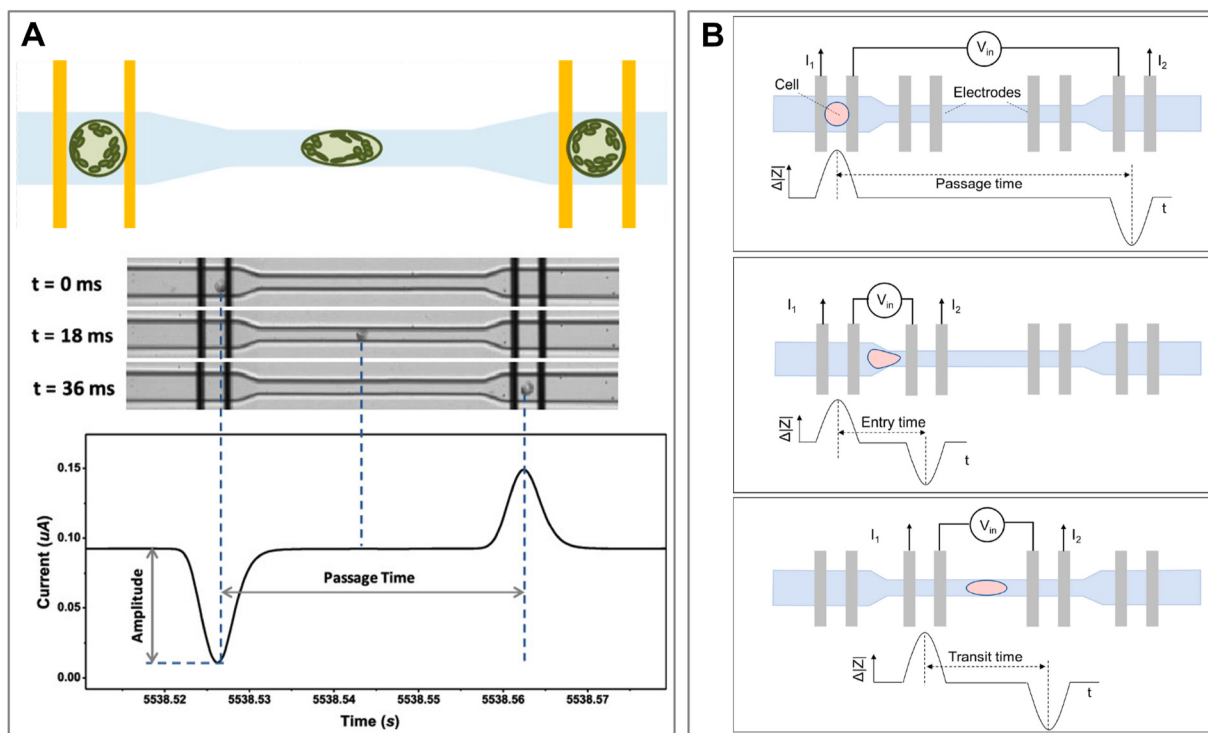


**Fig. 8.** (A–B) Designs for electrical impedance and mechanical characterization. (A) Reprinted with permission from Ref. [94]. Copyright 2020, American Chemical Society. (B) Reprinted with permission from Ref. [95]. Copyright 2018, American Chemical Society.

sensitivity. However, this usually requires more time-consuming and complex data-processing steps.

### 3.3. Other two-dimensional electrodes

Afshar et al. presented dual-frequency dielectrophoresis (DEP) cytometry to measure and monitor membrane capacitance and cytoplasmic conductivity changes in Chinese hamster ovary (CHO) cells

during starvation-induced apoptosis (Fig. 9A) [96]. In this device, the exciting electrodes  $A_1$  and  $A_2$  were supplied with a voltage at two selected DEP frequencies  $f_1$  and  $f_2$  to generate a DEP force on the flowing cells. The DEP force can induce a change in the cell position along the vertical direction of the channel, and the change in cell position can be detected by the sensing electrodes  $S_1$ ,  $S_2$ , and  $S_3$  located on either side of the exciting electrodes. The exciting electrodes and sensing electrodes were separated by ground electrodes (continuous S-shaped) to shield the

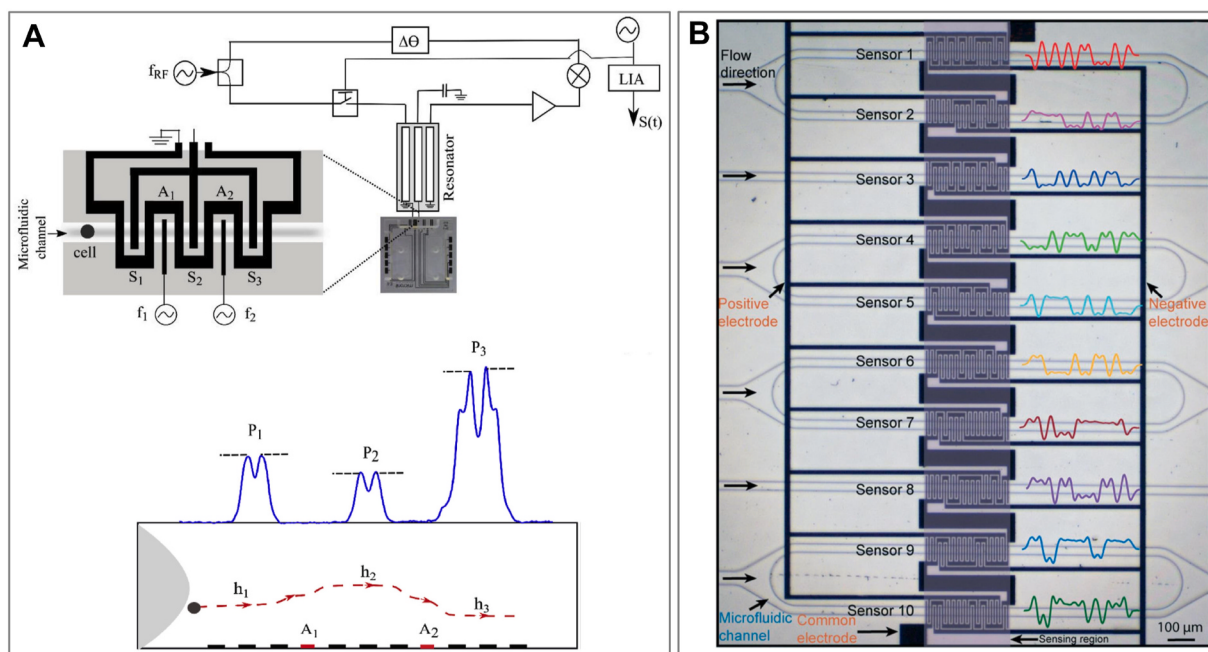


**Fig. 9.** (A) The dual-frequency DEP cytometer. Reprinted with permission from Ref. [96]. Copyright 2019, Elsevier. (B) The code-multiplexed Coulter sensor network. Reprinted with permission from Ref. [97]. Copyright 2019, Royal Society of Chemistry.

cross current. As the cell flows over the sensor zone, the cell heights  $h_1$ ,  $h_2$ , and  $h_3$  were related to the DEP force acting on the cell, which can be measured from the shape and magnitude of the response signals. The DEP force was influenced by cell membrane capacitance and cytoplasm conductivity; thus, different types of cells could be differentiated by analyzing the height of cells above the electrode zone. This device, which couples MIC with the DEP technique, realized the monitoring of cell membrane capacitance and cytoplasm conductivity. However, the sensing throughput of this device was limited by the weak DEP force. In addition, to track particles in multiple channels using simple hardware, Wang et al. proposed a code-multiplexed Coulter sensor network (Fig. 9B) [97]. The coded counter sensors with unique electrode patterns were placed under the corresponding channels separately, which can produce location-specific electrical waveforms as particles flowing through different channels. Then, the particle trajectory information can be extracted by analyzing the waveforms via a deep learning-based algorithm that employs ConvNets. Therefore, this device offers a fast and simple method for multichannel and high-throughput cell sensing. In their more recent work, an error correction technique that was used in telecommunication systems for controlling errors in data over unreliable communication channels was combined with a more simple code-multiplexed Coulter sensor network, achieving multichannel cell sensing as well [98].

#### 4. Three-dimensional electrode

##### 4.1. Facing electrode configuration

The three-dimensional facing electrode configuration usually

contains facing electrode arrays, and the electrodes are located at the top and bottom of the channel separately. Compared to the two-dimensional electrode, the electric field distribution between parallel-facing electrodes is more homogeneous (although not completely uniform), which is more suitable for highly sensitive impedance detection [99]. Typically, an AC voltage is applied to the top electrodes, which are used as excitation electrodes, while the bottom electrodes serve as sensing electrodes for receiving response signals. The principle for cell sensing is similar to the aforementioned two-electrode configuration, where the current change upon passage of the cell between the facing electrodes is recorded and then calculated to acquire the cell information. It was noted that the nonuniformity of the electric field still exists, because the intensity of the electric field near the exciting electrode is stronger than that near the sensing electrode, and thus the particle position in the channel still affects the impedance signals. To overcome this issue, researchers focused cells into the central line of the channel before entering the parallel facing electrode zone. For instance, Haandbaek et al. designed an impedance cytometer that integrates a pair of electrodes for DEP focusing of the cells, as well as a pair of facing electrodes for cell sensing (Fig. 10A) [100]. Moreover, to improve the sensitivity of the impedance changes, an electrical resonator was serialized into this MIC device. At resonance, the impedance of the series resonance circuit was very low, resulting in a high response current, thereby enhancing the sensing sensitivity. As shown in Fig. 10A, the slope of the signal magnitude curve is close to zero at frequencies close to resonance, causing poor signal magnitude sensitivity in this region. In contrast, the signal phase sensitivity was large in this region owing to the largest slope of the magnitude curve at resonance. Therefore, by primarily using the phase information, this device displayed better sensitivity to changes in

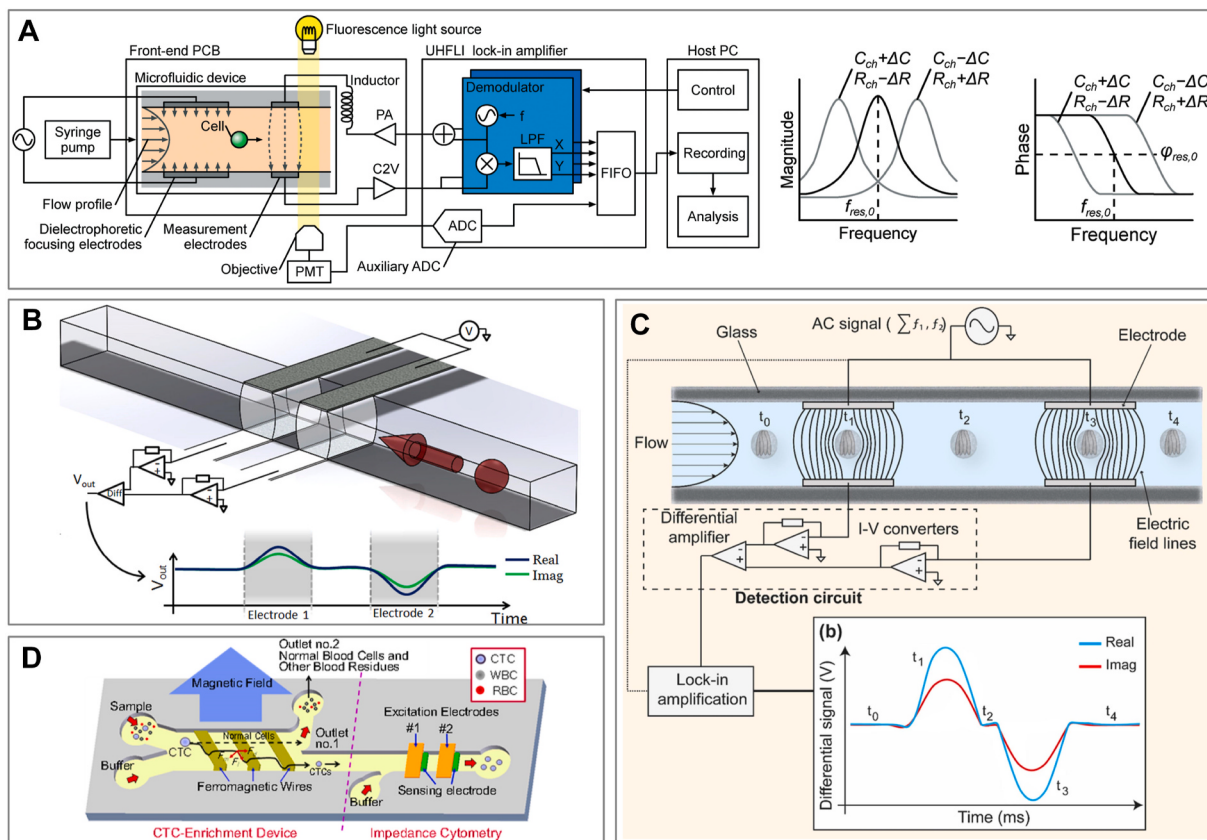


**Fig. 10.** (A) The MIC device integrated DEP focusing electrodes and a pair of facing electrodes. Reprinted with permission from Ref. [100]. Copyright 2014, Royal Society of Chemistry. (B) Two pairs of facing electrodes for differential measurement. Reprinted with permission from Ref. [104]. Copyright 2014, American Institute of Physics. (C) The facing electrodes for identification and viability detection of protozoan pathogens. Reprinted with permission from Ref. [105]. Copyright 2017, Springer Nature. (D) A two-step platform that coupled a CTC-enrichment and MIC device for simultaneous separation and detection of CTCs. Reprinted with permission from Ref. [109]. Copyright 2015, American Chemical Society.

impedance than other similar devices [101], and first achieved the discrimination of single *Escherichia coli* and *Bacillus subtilis* cells. Later, researchers proposed a differential measurement scheme based on two pairs of facing electrodes [102,103]. In this configuration, the two top electrodes were used as exciting electrodes, whereas the two bottom electrodes were used as sensing electrodes to obtain differential signals. As explained in Section 3.2, the differential signals offer the advantages of low background noise and high sensing sensitivity. In the past ten years, two pairs of parallel facing electrodes have been the most commonly used structures in MIC devices. For instance, Spencer et al. used two pairs of parallel facing electrodes to differentiate MCF-7 cells from large background leukocytes (Fig. 10B) [104]. McGrath et al. identified and evaluated the viability of protozoan pathogens (such as single *Cryptosporidium parvum* and *C. muris* oocysts, and *Giardia lamblia*

cysts) by using similar structures (Fig. 10C) [105]. Compare to two-dimensional co-planar electrode configurations, facing electrode configuration typically owns a high sensing accuracy and can be used in cell drug exposure tests. For example, to meet the need for controlling cellular composition during organoid formation from coax human-induced pluripotent stem cells, Honrado et al. used the two pairs of parallel facing electrodes configuration to quantify the cell sub-populations under camptothecin doses used to arrest the cell cycle [106]. To further improve the sensitivity of their device, the impedance signal of individual cells was normalized using standard polystyrene beads, by dividing all impedance data by the mean impedance data of standard beads. As the high sensitivity of this electrode configuration, bacteria with small size can also be detected and monitored. For example, Clausen et al. distinguished different impedance signals for 1

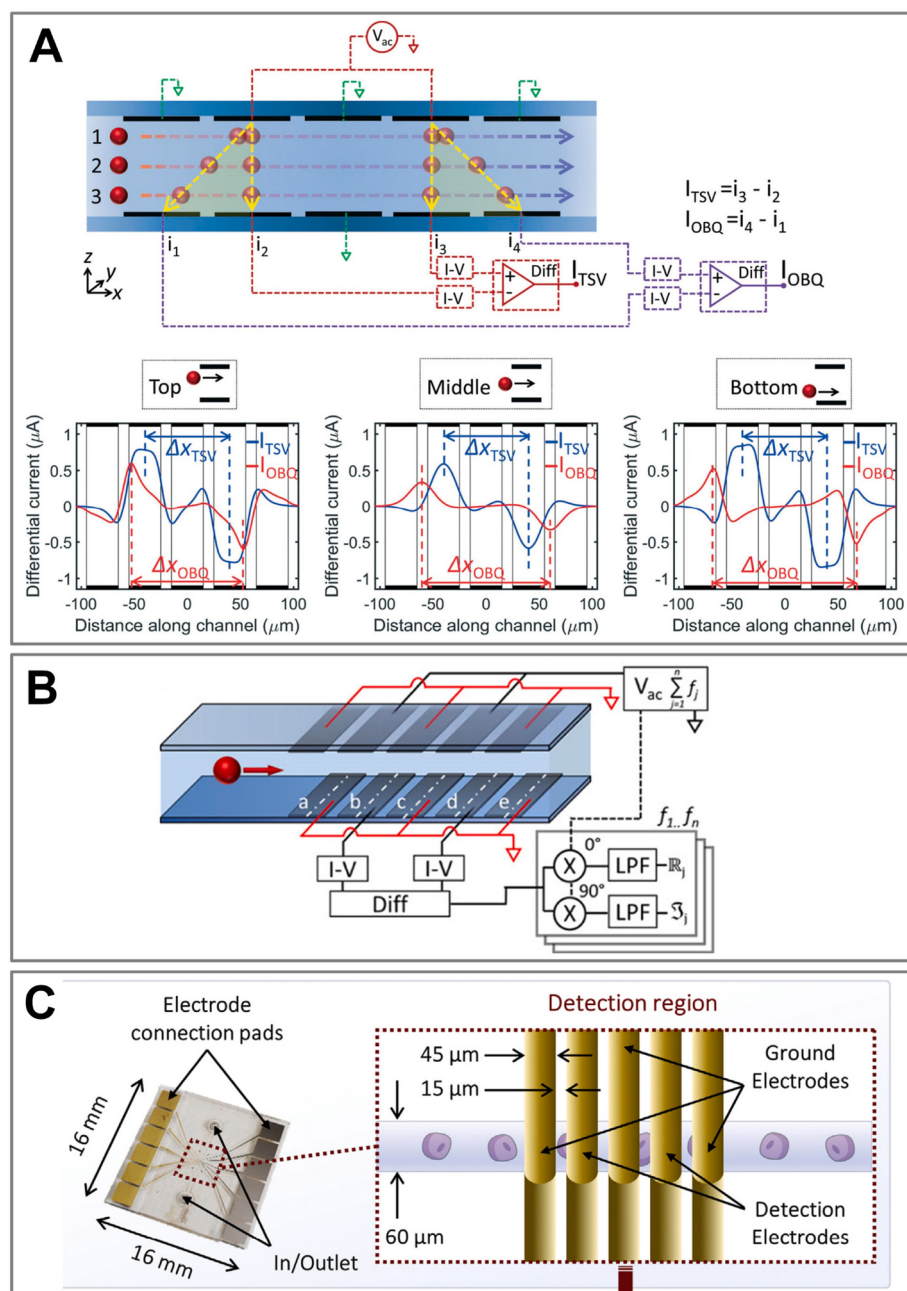


**Fig. 11.** (A) Five pairs of facing electrodes enabling transverse and oblique differential current measurements. Reprinted with permission from Ref. [113]. Copyright 2016, Royal Society of Chemistry. (B–C) Structure and application of the five pairs of facing electrode configurations. (B) Reprinted with permission from Ref. [114]. Copyright 2020, American Chemical Society. (C) Reprinted with permission from Ref. [115]. Copyright 2020, Elsevier.

and 2  $\mu\text{m}$  particles, as well as *Escherichia coli* and *S. aureus* bacteria [107]. Moore et al. achieved the identification for the phenotype of *Clostridioides difficile* bacteria in its vegetative form [108]. Researchers have also integrated the microfluidic cell sorting method with two pairs of parallel-facing electrodes. For example, Han et al. developed a two-step platform that coupled a CTC-enrichment device and impedance cytometry for the simultaneous separation and detection of CTCs [109]. Rare CTCs were separated from normal blood cells and unwanted debris through immunomagnetic nanobeads (MNB) and lateral magnetoporesis (Fig. 10D). Then, the separated CTCs were coated with graphene nanoplates (GNPs) before entering the detection zone to increase the electrical differentiation accuracy. Since the CTCs covered by GNPs have higher conductivity than normal blood cells, the GNP-coated CTCs could generate a greater electrical impedance difference compared to normal cells. Moreover, researchers have integrated the two pairs of facing electrodes with other modules to achieve multiple parameter detection of cells [39]. For instance, Haandbaek et al. combined this configuration with a high-speed camera to characterize the physical morphology of a single cell in parallel with its dielectric properties [110]. By using this device, the *Saccharomyces cerevisiae* species as either single or budding cells could be classified.

In two or more pairs of parallel-facing electrodes, the non-homogeneity of the electric field and diagonal current flow between the diagonal electrodes result in the variation of the impedance signal according to the particle positions [111]. Researchers have demonstrated that increasing the distance between electrodes in the same plane or decreasing the dimension of the channel can alleviate the positional dependence of impedance, but at the expense of poor sensitivity or low throughput [112]. To overcome these drawbacks, a signal-processing compensation strategy was introduced into the facing electrode configuration. For instance, Spencer et al. proposed five pairs of facing electrode configurations, realizing high-quality impedance signals under relatively high throughput [113]. As shown in Fig. 11A, an AC voltage was applied to the two top electrodes, and two differential signals, transverse and oblique, were acquired using four bottom electrodes. Four ground electrodes were used to reduce the magnitude of the cross current and the errors in the impedance signals. It was noted that peak-to-peak time in oblique and transverse current signals reflect particle heights and flow rates; their ratio only depends on particle heights, which can be used to estimate the vertical position of particles and correct the impedance signals for off-center particles. This technique can differentiate 5, 6, and 7  $\mu\text{m}$  particles without focusing, and provides an excellent particle size coefficient of variation. Although this signal-processing compensation strategy eliminates the positional dependence of the signal, it requires a relatively significant computational overhead for large data post-processing. To overcome this drawback, this research group redesigned this electrode configuration, which allows real-time impedance analysis of particles [114]. As illustrated in Fig. 11B, three pairs of non-signal electrodes were connected to the ground to minimize the current leakage of nearest-neighbor signal electrodes, which can eliminate impedance errors for off-center particles, and avoid the post-processing overhead of the signal-processing compensation strategy. In addition, unlike existing techniques that measure a single cell at one or two simultaneous frequencies, this device measured eight simultaneous frequencies to acquire the complete intrinsic electric properties of thousands of single cells in a short time. The applicability of this study was to obtain the full frequency-dependent properties of RBCs and red cell ghosts (no hemoglobin in the cytoplasm). Moreover, McGrath et al. applied five similar pairs of parallel facing electrode configurations to evaluate the tumorigenicity of pancreatic ductal adenocarcinoma (PDAC) (Fig. 11C) [115]. They proposed a novel phase contrast metric that exhibits variations in the high-and low-frequency impedance phase responses to show systematic differences in the electrophysiology of the cell interior, which is found to be related to the tumorigenicity of cells.

In addition, Caselli et al. developed a novel wiring scheme for two

conventional pairs of parallel facing electrodes [116], enabling high-accuracy cell sensing without resorting to particle focusing. Instead of applying the AC voltage on the same side of the facing electrode configuration and acquiring the differential current signal on the other side, this scheme applied the AC voltage to diagonally opposite electrodes and collected the differential current signal on the remaining electrodes. As shown in Fig. 12A, a particle flowing in the lower half of the channel (trajectory 1) was closer to the sensing electrode of the left pair of electrodes and exciting electrodes of the right pair of electrodes. Accordingly, the left half of the recorded signal had a higher amplitude than that of the right half. The opposite behavior was presumed when the particle flowed through the higher half of the channel (trajectory 3), which indicates that the signal amplitude difference is affected by the particle trajectory height. Similar to the aforementioned signal compensation strategies, the left-right asymmetry of the differential current signal was used to compensate impedance errors for off-center particles [37,113]. This method has the advantages of a simple structure and high detection accuracy, and impedance data for 5.2, 6, and 7  $\mu\text{m}$  particles were obtained with a coefficient of variation similar to those provided by the suppliers. Later, Spencer et al. followed and improved this wiring scheme in their device [117], enabling simple and fast antimicrobial susceptibility tests (Fig. 12B). Briefly, four pairs of parallel-facing electrodes were set in the detection zone, and the adjacent pairs of parallel-facing electrodes were applied with AC voltages with the same amplitude and opposite phase. Furthermore, the phases of currents in the left or right two pairs of electrodes were opposite, and thus reduced the baseline current (no cell). After the difference in current signals between the left and right half electrodes, this method allowed a higher amplifier and SNR than other MIC devices, and enabled a limited detection of  $\sim 400$  nm radius bio-particles. Using this device, the phenotypic response of the bacteria to the mode of action of a particular antibiotic could be measured in a label-free manner. For example, the minimum inhibitory concentration of carbapenem-resistant *Klebsiella pneumoniae* can be measured.

As the most popular type of three-dimensional electrode, the facing electrode configuration has high sensing accuracy. By using the signal compensation strategies or optimized electrode design, bio-particles as small as 400 nm in diameter can be successfully detected. However, in many biomedical applications (such as identifying CTCs from the blood of a patient with cancer), the detection throughput is relatively low, and a device that parallels multiple facing electrode configurations to meet this requirement has not yet been developed. Moreover, because precise alignment is required in the fabrication process, there is an urgent need to develop a simpler fabrication method to achieve more widespread use.

#### 4.2. Special three-dimensional electrode configuration

To simplify the fabrication process of three-dimensional electrodes, many special three-dimensional electrode configurations have been proposed. For instance, Yang et al. used a low-melt-point alloy to fabricate self-aligned 3D electrodes in their microfluidic biophysical phenotyping device (Fig. 13A) [118]. Alloy wires (melting point 60 °C) were inserted into the pre-fabricated electrode channel, and then the alloy wires were heated to melt, and then the whole electrode channels were filled through capillary forces to form 3D electrodes. There are two fluidic channels, both of which consist of four successive constrictions and three relaxation regions. The 3D electrodes directly contacted the two fluidic channels for differential electrical impedance measurement. When a single cell passes through the constriction and relaxation regions, the squeeze of the cell in the constriction regions blocks the electrical field lines, thereby increasing the impedance signal. The transit time of a single cell passing through each constriction reflected cell deformability, whereas the magnitude of the impedance signal was dependent on the electrical properties of the cell. Therefore, cytochalasin B-treated and N-ethylmaleimide-treated MCF-7 cells could be

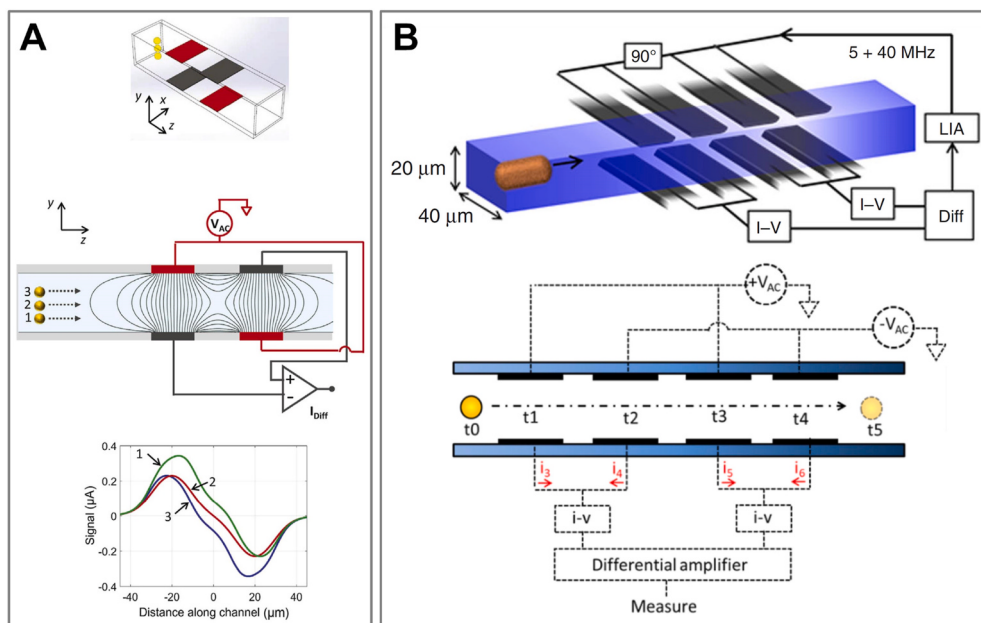


**Fig. 12.** (A–B) The wiring schemes for facing electrode configurations. (A) Reprinted with permission from Ref. [116]. Copyright 2018, Elsevier. (B) Reprinted with permission from Ref. [117]. Copyright 2020, Springer Nature.

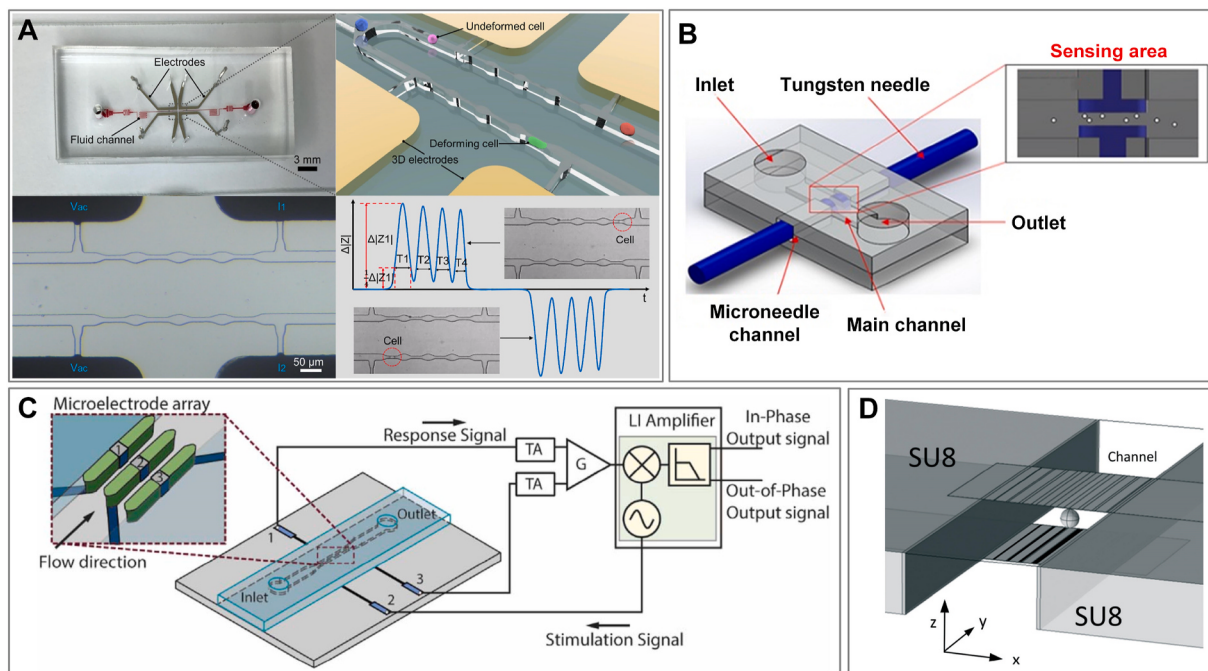


**Fig. 13.** (A) The self-aligned 3D electrodes made of low melt point alloy. Reprinted with permission from Ref. [118]. Copyright 2019, Elsevier. (B) Three-dimensional electrode fabricated by inserting two reusable microneedles into both sides of the channel. Reprinted with permission from Ref. [119]. Copyright 2017, Multidisciplinary Digital Publishing Institute. (C) Three 3D free-standing electrodes embedded in a channel for generating a uniform electric field. Reprinted with permission from Ref. [120]. Copyright 2017, Elsevier. (D) Two facing electrode arrays with gradually increasing conductive area. Reprinted with permission from Ref. [121]. Copyright 2019, Royal Society of Chemistry.

differentiated based on their biophysical properties. In addition, they used a trained neural network to further increase the accuracy and sensitivity of the device. In a recent study, researchers inserted two reusable microneedles into both sides of the channel to form a three-dimensional electrode configuration (Fig. 13B) [119]. The detection principle was the same as that of the two-electrode MIC device. Using this device, the cell concentrations of yeasts could be measured at frequencies ranging from 100 kHz to 5 MHz. These fabrication

technologies offer a simple and low-cost method for three-dimensional electrodes, but also suffer from the disadvantages of a larger electrode volume and low fabrication accuracy. In addition, an MIC device that embedded three 3D free-standing electrodes in a channel was proposed by Rollo et al. [120]. The faces of these electrodes were aligned to the flow direction, which generates a uniform electric field for cell sensing (Fig. 13C). This device was employed to assess the impedance change associated with T cell activation at the electric frequency. However, it is

noteworthy that the electrode gaps should be carefully determined to avoid clogging. To track the particle position in microfluidic channels, Solsona et al. created a gradually increasing conductive area on the two facing electrode arrays (Fig. 13D), hence generating a non-homogeneous electric field at low frequencies ( $\sim 800$  Hz) [121]. Particles located in the low electric field intensity region would generate lower signal amplitudes than those in the high electric field region; thus, it could deduce the position of the particles. At high frequencies ( $\sim 100$  kHz), the electric field was homogeneous, because the impedance of all the capacitors was much smaller than that of the medium; therefore, the conductivity of the particles and system can be measured. This device offers a new method for particle trajectory measurement, which is promising for signal compensation and increases detection accuracy.

## 5. Liquid electrode

Metal electrodes often require complex fabrication and assembly processes, whereas liquid electrodes use conductive liquids to form detection electrodes. Coulter counter, as the classical single-cell detector, can be regarded as a liquid electrode used [122–124]. As shown in Fig. 14A, two chambers filled with conductive liquid were connected by an orifice. Two metal wires with DC voltage were separately positioned at both sides of an orifice. Cells passing through this orifice displace the original conductive fluid and alter the resistance, which is measured as a current pulse. A limitation of the classical Coulter counter is that DC resistance measurements only provide information regarding cell size and number. Later, based on this design, Hoffman et al. achieved AC impedance measurement of cells at multiple frequencies (100 kHz–50 MHz), which can obtain exhaustive information regarding cells [125]. However, the orifice is typically larger than the cell size in conventional Coulter counters, resulting in current leakage where the electric current circumvents the measured cells, which makes the measurement unreliable. To overcome this hurdle, a constriction channel design was composed to the microfluidic flow cytometer, enabling the accurate measurement of cell elongation and impedance profiles [59]. From Fig. 14B, as the single cells were aspirated through the constriction channel, it fully blocked the electric field and generated an impedance signal. The cell transit time through the constriction region as well as the impedance amplitude were used to reveal cell elongation and electric properties, which can be used to classify different cell populations, such

as bone cells of osteoblasts and osteocytes. In addition, Chiu et al. also used a similar structure to identify EpCAM-positive CTCs from surrounding EpCAM-negative cells [126], but used a capillary tube to transfer cells directly into the constriction channel to increase the utilization of the cell sample (Fig. 14C). In a more recent study, Zhang et al. reported a multiple-pore-based microfluidic Coulter counter to improve the detection accuracy (Fig. 14D) [127]. When a single particle passed through an array of constriction pores, the particle was detected multiple times, and multiple time-related resistive pulse signals were generated. These signals were analyzed using the multiple cross-correlation analysis (MCCA) method, which demonstrated that the sizing SNR can be amplified by  $\sqrt{n}$  ( $n$  is the number of constriction pores). This concept was successfully verified by the detection of standard beads and human RBCs. Because of the small size of the sensing orifice, most Coulter counter-based devices usually suffer from the drawbacks of low throughput and easy clogging. As a result, Choi et al. reported a microfluidic time-division multiplexing accessing (TDMA) single-end pulse sensor [128], where particles can be measured simultaneously by multiple channels (Fig. 14E). Using this method, the particle size and concentration can be calculated using eight channels simultaneously.

Tang et al. developed an impedance microcytometer that integrates inertial focusing and a pair of perpendicularly positioned liquid electrodes to the sample flow (Fig. 15A) [48]. The liquid electrodes were constructed by inserting AgCl wires into a highly conductive electrolyte solution. When a focused cell flows through the sensing zone, the detection sensitivity can be easily enhanced by decreasing the length of the sensing zone by increasing the flow rate of the conductive electrolyte solution. Based on this device, they achieved a high detection throughput of  $\sim 5000$  cells/s and differentiated the MCF-7 and WBCs according to the width and amplitude of the response signals. In addition, a liquid electrode can also be created through a coplanar metal electrode. For instance, as shown in Fig. 15B, researchers positioned two coplanar metal electrodes at the bottom of the lateral channel perpendicular to the main channel [129]. This configuration could create a homogeneous electric field over the main channel height by the conductive liquid. Similarly, researchers inserted two gold pins in both sides of the detection channel, two perpendicular channels filled with conductive media connected them, thereby forming liquid electrodes (Fig. 15C) [130]. This device achieved the identification of 7.66, 10.5,

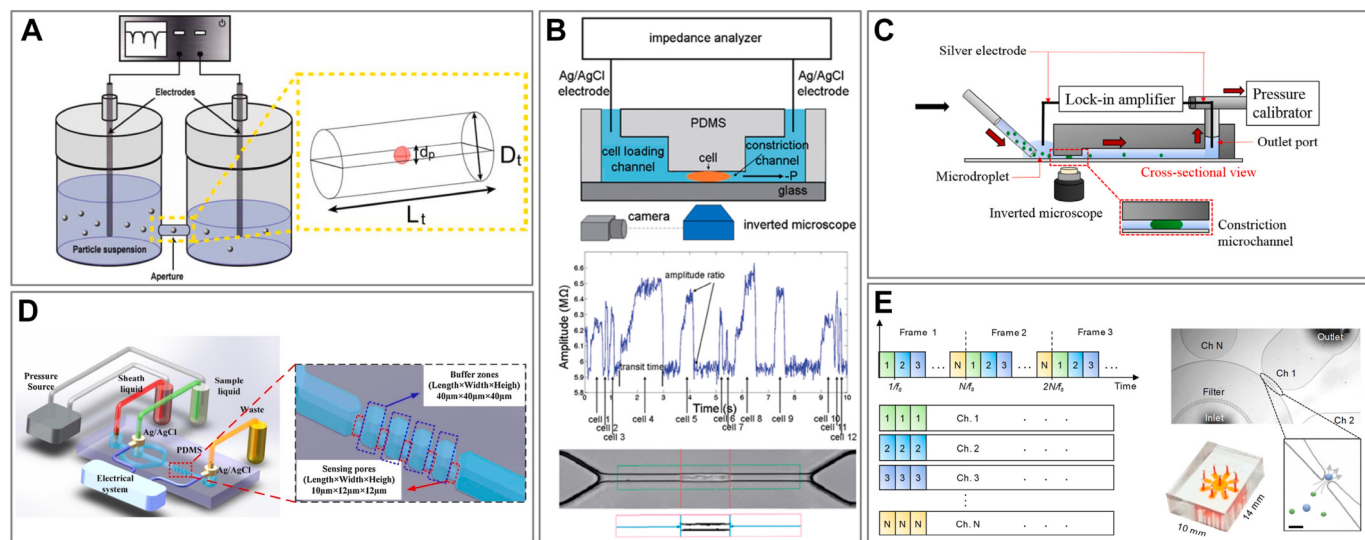


**Fig. 14.** (A) The working principle of a Coulter counter. Reprinted with permission from Ref. [49]. Copyright 2010, Springer Nature. (B–C) A constriction channel design for decreasing current leakage. (B) Reprinted with permission from Ref. [59]. Copyright 2011, Royal Society of Chemistry. (C) Reprinted with permission from Ref. [126]. Copyright 2017, Elsevier. (D) The multiple pore-based microfluidic Coulter counter. Reprinted with permission from Ref. [127]. Copyright 2019, Elsevier. (E) The microfluidic TDMA single-end pulse sensor for measuring multiple channels simultaneously. Reprinted with permission from Ref. [128]. Copyright 2019, American Chemical Society.

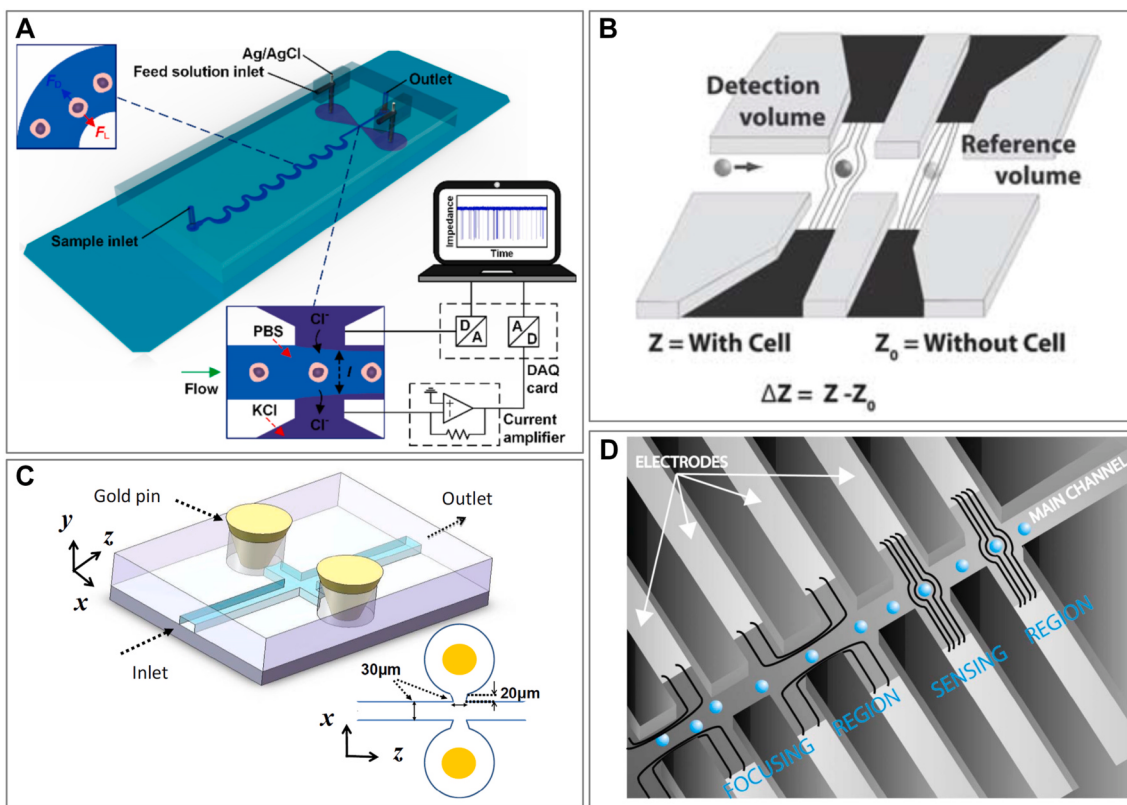


**Fig. 15.** (A) A pair of perpendicular positioned liquid electrodes to the sample flow for cell sensing. Reprinted with permission from Ref. [48]. Copyright 2017, American Chemical Society. (B) Liquid electrode fabricated by using coplanar electrodes and conductive liquid. Reprinted with permission from Ref. [129]. Copyright 2010, Royal Society of Chemistry. (C) Liquid electrode fabricated by using gold pins and conductive liquid. Reprinted with permission from Ref. [130]. Copyright 2016, American Institute of Mathematical Sciences. (D) Liquid electrode integrated with DEP focusing unit. Reprinted with permission from Ref. [131]. Copyright 2012, Royal Society of Chemistry.

and 14.7  $\mu\text{m}$  particles successfully. Furthermore, DEP focusing unit could also be integrated with liquid electrode configuration to ensure the consistency of the response signal (Fig. 15D) [131]. However, to generate a uniform electric field, the distance between metal electrodes on both sides of the detection channel needs to be sufficiently large, resulting in poor sensitivity of these liquid electrode configuration.

A liquid electrode configuration is usually able to create a continuous large-area homogenous electric field. This feature allows the liquid electrode to produce a larger detection area for cell sensing. In addition, because precise metal electrode fabrication processes are not required, the liquid electrode can be fabricated easily. However, this configuration typically suffers from the disadvantages of poor cell sensing sensitivity owing to instability when the conductive liquid flows in the channel.

## 6. Conclusion and outlook

Over the past two decades, microfluidic impedance cytometry has shown its ability to differentiate cells based on their inherent features (such as size, shape, and dielectric properties), and has been developing effective POC diagnostic devices. Because MIC devices have the advantages of simple structure, small footprint, high sensitivity, and low reagent consumption, these devices are superior to other technologies with respect to mass production and integration with other functional modules. In recent years, the development and advancement of many novel electrode structures to create new MIC devices have achieved higher sensing sensitivity, higher throughput, and more comprehensive biochemical applications. In this review, we presented a general view of electrode design and its development in MIC devices (Table 1). Different from previous reviews, our review is a comprehensive review that

focuses on the influences of various electrode configurations (two-dimensional, three-dimensional, and liquid electrodes) on cell sensing.

In terms of sensing accuracy, the uniformity of the electric field distribution plays the most important role. According to recent studies, the parallel-facing electrode configuration provides a more uniform electric field than other configurations. Bio-particles as small as 400 nm can be detected using this configuration, which is difficult to achieve using other electrode configurations. However, there is a higher requirement for sensing accuracy in biomedical applications, such as drug exposure and bacterial or viral infections. To further improve the sensing accuracy, the electrode design should focus on generating a more uniform electric field. Advanced simulation methods and tools offer a convenient way to verify the uniformity of newly designed electrode structures, instead of using time-consuming and laborious trial-and-error methods. A useful software, named "COMSOL," has been developed as a powerful multi-physics field simulation software for simulating the electric field distribution of designed electrode structures, allowing researchers to optimize it in a short time. In the future, advanced models and software that can simulate the electric field distribution and guide electrode design are still required. In addition, focusing units that are used to ensure consistency in the particle positions can also increase impedance sensing accuracy. A detailed discussion on this aspect has been provided in recent reviews [33,36].

The signal correction methods (such as the compensation strategy used in five pairs of facing electrodes) applied in different electrode configurations can compensate to a certain extent for the detection errors caused by the nonuniformity of the electric field, thereby improving the sensing sensitivity. In addition, the aforementioned signal processing methods, such as the Bayesian approach, can enhance the impedance detection throughput. However, many devices using these methods can

**Table 1**

Overview of various types of electrode configurations for MIC devices.

Configuration	Number of electrodes	Application	Reference
Two-electrode configuration	2	Bare magnetic beads and tumor cells differentiation	Lin et al. Ref. [65]
Two-electrode configuration embedded with constricted channel	2	Yeast budding analysis	Xie et al. Ref. [71]
Three-electrode configuration integrated with inertial spiral microfluidics	3	Tumor cells and RBCs differentiation	Desai et al. Ref. [78]
Three-electrode configuration integrated with inertial spiral microfluidics	3	Diabetes testing	Petchakup et al. Ref. [81]
Three-electrode configuration embedded with constricted channel	≥3	Tumor cell identification	Zhou et al. Ref. [95]
Facing electrode configuration combined with DEP focusing unit	2	<i>Escherichia coli</i> and <i>Bacillus subtilis</i> classification	Haandbaek et al. Ref. [100]
Facing electrode configuration with two pairs of electrodes	4	Viability evaluation of protozoan pathogens	McGrath et al. Ref. [105]
Facing electrode configuration with five pairs of electrodes	10	Red cell ghosts and RBCs identification	Spencer et al. Ref. [114]
Four pairs of parallel-facing electrodes with a novel wiring scheme	8	Measurement of minimum inhibitory concentration for carbapenem-resistant <i>Klebsiella pneumoniae</i>	Spencer et al. Ref. [117]
Coulter counter with multiple detection pores	–	Standard beads and RBCs detection	Zhang et al. Ref. [127]
Liquid electrode configuration using highly conductive electrolyte solution	–	MCF-7 and WBCs classification	Tang et al. Ref. [48]

only obtain relatively simple cell information, such as size and number. In the future, more specific data analysis methods should be used to extract more rich cell information. In many clinical applications, such as identifying CTCs from the blood of patients with cancer, there is an urgent need to realize real-time detection with ultra-high throughput. Multi-channel impedance sensing is promising for meeting these requirements. However, the scalability of channel numbers is limited because each channel needs an independent signal input/output instrument. To address this issue, frequency division multiple access (FDMA) [132], code-division multiple access (CDMA) [98], and TDMA methods could be used in MIC devices with multi-channel for processing the multiplexing signals [128].

Although MIC devices can offer rich information on cell phenotype in a label-free manner, the sensitivity and specificity are far from those of commercial flow cytometry using fluorescent antibody labeling techniques. For example, the current MIC devices cannot differentiate between different antigen-expressing cell subtypes with similar sizes and shapes. To overcome this issue, different electrode configurations can be integrated to obtain more cell information, such as cytoplasm conductivity and nucleus size, which can be used for more precise cell classification. Moreover, cell morphology and refractive index detection through optical modules, cell deformability detection through acoustics or optical modules, as well as other noninvasive detection modules, can also be introduced to these devices to realize the multi-parameter detection of cells. This may be due to the tendency to use MIC devices

for label-free and noninvasive detection.

To realize POC applications, MIC devices should be inexpensive and easily fabricated. However, current electrode fabrication methods are time-consuming and complex. For example, the facing electrode configuration usually requires complex photolithography processes and precise alignment of the upper and lower electrodes. In addition, the bonding between parallel facing electrodes typically depends on the photoresist, resulting in weak bonding; thus, it has a relatively high defect rate. Therefore, these drawbacks limit their extensive application and further advancement. Laser writing in conductive films, inkjet printing electrodes, and 3D printing technologies may be able to address these problems. Although these technologies are limited by their relatively low fabrication accuracy, their potential for fabricating electrodes has not been fully developed.

In summary, although microfluidic impedance cytometry has undergone great advances over the past few years, further development is urgently needed to simplify fabrication processes, increase detection accuracy and throughput, improve real-time and continuous detection, and acquire rich information regarding cells. The advancement and development of electrode configurations play a vital role in these requirements; thus, more studies should be focused on this aspect. It is envisioned that, with the update of fabrication technologies, software, and electronic hardware, MIC devices have a bright future.

#### Declaration of competing interest

The authors declare that they have no known competing financial interests or personal relationships that could have appeared to influence the work reported in this paper.

#### Acknowledgements

This research work is supported by the National Natural Science Foundation of China (81727801, 51875103 and 51775111), the Natural Science Foundation of Jiangsu Province (BK20190064), the Six Talent Peaks Project of Jiangsu Province (SWYY-005), the Zhishan Youth Scholar Program of SEU, and the Jiangsu Graduate Innovative Research Program (KYCX20\_0083).

#### References

- [1] M. Barreiros Dos Santos, R.B. Queiros, A. Geraldes, C. Marques, V. Vilas-Boas, L. Dieguez, E. Paz, R. Ferreira, J. Morais, V. Vasconcelos, J. Piteira, P.P. Freitas, B. Espina, Portable sensing system based on electrochemical impedance spectroscopy for the simultaneous quantification of free and total microcystin-LR in freshwaters, Biosens. Bioelectron. 142 (2019) 111550.
- [2] H.E. Kubitschek, Electronic counting and sizing of bacteria, Nature 182 (1958) 234–235.
- [3] E.P. Preece, F.J. Hardy, B.C. Moore, M. Bryan, A review of microcystin detections in Estuarine and Marine waters: environmental implications and human health risk, Harmful Algae 61 (2017) 31–45.
- [4] M.F. Abate, M.G. Ahmed, X.R. Li, C.Y. Yang, Z. Zhu, Distance-based paper/PMMA integrated ELISA-chip for quantitative detection of immunoglobulin G, Lab Chip 20 (2020) 3625–3632.
- [5] Y. Chen, J. Peng, Y. Lai, B. Wu, L. Sun, J. Weng, Ultrasensitive label-free detection of circulating tumor cells using conductivity matching of two-dimensional semiconductor with cancer cell, Biosens. Bioelectron. 142 (2019) 111520.
- [6] X. Wu, Y. Xia, Y. Huang, J. Li, H. Ruan, T. Chen, L. Luo, Z. Shen, A. Wu, Improved SERS-active nanoparticles with various shapes for CTC detection without enrichment process with supersensitivity and high specificity, ACS Appl. Mater. Interfaces 8 (2016) 19928–19938.
- [7] D.C. Grulke, N.A. Marsh, B.A. Hills, Experimental air-embolism - measurement of microbubbles using coulter counter, Br. J. Exp. Pathol. 54 (1973) 684–691.
- [8] Y. Husemann, J.B. Geigl, F. Schubert, P. Musiani, M. Meyer, E. Burghart, G. Forni, R. Eils, T. Fehm, G. RiethmUller, C.A. Klein, Systemic spread is an early step in breast cancer, Canc. Cell 13 (2008) 58–68.
- [9] I.M. London, D. Shemin, R. West, D. Rittenberg, Heme synthesis and red blood cell dynamics in normal humans and in subjects with polycythemia vera, sickle-cell anemia, and pernicious anemia, J. Biol. Chem. 179 (1949) 463–484.
- [10] Y. Katsumoto, K. Tatsumi, T. Doi, K. Nakabe, Electrical classification of single red blood cell deformability in high-shear microchannel flows, Int. J. Heat Fluid Flow 31 (2010) 985–995.

- [11] P.K. Lam, T.V. Ngoc, T.T.T. Thuy, N.T.H. Van, T.T.N. Thuy, D.T.H. Tam, N. M. Dung, N.T.H. Tien, N.T.T. Kieu, C. Simmons, B. Wills, M. Wolbers, The value of daily platelet counts for predicting dengue shock syndrome: results from a prospective observational study of 2301 Vietnamese children with dengue, *PLoS Neglected Trop. Dis.* 11 (2017), e0005498.
- [12] M.E. Piayena, S.W. Graves, The intersection of flow cytometry with microfluidics and microfabrication, *Lab Chip* 14 (2014) 1044–1059.
- [13] M.I. Lapsley, L. Wang, T.J. Huang, On-chip flow cytometry: where is it now and where is it going? *Biomarkers Med.* 7 (2013) 75–78.
- [14] M. Reisbeck, L. Richter, M.J. Helou, S. Arlinghaus, B. Anton, I. van Dommelen, M. Nitzsche, M. Bassler, B. Kappes, O. Friedrich, O. Hayden, Hybrid integration of scalable mechanical and magnetophoretic focusing for magnetic flow cytometry, *Biosens. Bioelectron.* 109 (2018) 98–108.
- [15] H. Yan, Y. Wu, Y. Zhou, M. Xu, P. Paiè, C. Lei, S. Yan, K. Goda, Virtual optofluidic time-stretch quantitative phase imaging, *APL Photonics* 5 (2020), 046103.
- [16] T. Gao, X. Gao, C. Xu, M. Wang, M. Chen, J. Wang, F. Ma, P. Yu, L. Mao, Label-free resistance cytometry at the orifice of a nanopipette, *Anal. Chem.* 93 (2021) 2942–2949.
- [17] S. Zhang, Z. Li, Q. Wei, Smartphone-based cytometric biosensors for point-of-care cellular diagnostics, *Nanotechnology and Precision Engineering* 3 (2020) 32–42.
- [18] J.B. Mitchell, K. McIntosh, S. Zvonic, S. Garretta, Z.E. Floyd, A. Kloster, Y. Di Halvorsen, R.W. Storms, B. Goh, G. Kilroy, X.Y. Wu, J.M. Gimble, Immunophenotype of human adipose-derived cells: temporal changes in stromal-associated and stem cell-associated markers, *Stem Cell.* 24 (2006) 376–385.
- [19] J. Cros, J. Raffenae, A. Couvelard, N. Pote, Tumor heterogeneity in pancreatic adenocarcinoma, *Pathobiology* 85 (2018) 64–71.
- [20] M. Ostermann, A. Sauter, Y. Xue, E. Birkeland, J. Schoelermann, B. Holst, M. R. Cimpan, Label-free impedance flow cytometry for nanotoxicity screening, *Sci. Rep.* 10 (2020) 142.
- [21] R. Nicolle, J. Raffenae, V. Paradis, A. Couvelard, A. de Reynies, Y. Blum, J. Cros, Prognostic biomarkers in pancreatic cancer: avoiding errata when using the TCGA dataset, *Cancers* 11 (2019) 126.
- [22] C. Honrado, P. Bisegna, N.S. Swami, F. Caselli, Single-cell microfluidic impedance cytometry: from raw signals to cell phenotypes using data analytics, *Lab Chip* 21 (2021) 22–54.
- [23] N. Nitta, T. Sugimura, A. Isozaki, H. Mikami, K. Hiraki, S. Sakuma, T. Iino, F. Arai, T. Endo, Y. Fujiwaki, H. Fukuzawa, M. Hase, T. Hayakawa, K. Hiramatsu, Y. Hoshino, M. Inaba, T. Ito, H. Karakawa, Y. Kasai, K. Koizumi, S. Lee, C. Lei, M. Li, T. Maeno, S. Matsusaka, D. Murakami, A. Nakagawa, Y. Oguchi, M. Oikawa, T. Ota, K. Shiba, H. Shintaku, Y. Shirasaki, K. Suga, Y. Suzuki, N. Suzuki, Y. Tanaka, H. Tezuka, C. Toyokawa, Y. Yaliqun, M. Yamada, M. Yamagishi, T. Yamano, A. Yasumoto, Y. Yatomi, M. Yazawa, D. Di Carlo, Y. Hosokawa, S. Uemura, Y. Ozeki, K. Goda, Intelligent image-activated cell sorting, *Cell* 175 (2018) 266–276.
- [24] Y. Fu, Q. Yuan, J. Guo, Lab-on-PCB-based micro-cytometer for circulating tumor cells detection and enumeration, *Microfluid. Nanofluidics* 21 (2017) 20.
- [25] B.C. Colson, A.P.M. Michel, Flow-through quantification of microplastics using impedance spectroscopy, *ACS Sens.* 6 (2021) 238–244.
- [26] T.R. Carey, K.L. Cotner, B. Li, L.L. Sohn, Developments in label-free microfluidic methods for single-cell analysis and sorting, *Wiley Interdisciplinary Reviews-Nanomedicine and Nanobiotechnology* 11 (2019) e1529.
- [27] A.B. Shrira, Z. Fritz, E.M. Novik, G.M. Yarmush, R.S. Schloss, J.D. Zahn, M. L. Yarmush, Microfluidic flow cytometry: the role of microfabrication methodologies, performance and functional specification, *Technology* 6 (2018) 1–23.
- [28] U. Abbasi, P. Chowdhury, S. Subramaniam, P. Jain, N. Muthe, F. Sheikh, S. Banerjee, V. Kumaran, A cartridge based Point-of-Care device for complete blood count, *Sci. Rep.* 9 (2019) 18583.
- [29] E.O. Adekanmbi, S.K. Srivastava, Dielectric characterization of bioparticles via electrokinetics: the past, present, and the future, *Appl. Phys. Rev.* 6 (2019), 041313.
- [30] F. Caselli, P. Bisegna, F. Maceri, EIT-inspired microfluidic cytometer for single-cell dielectric spectroscopy, *Journal of Microelectromechanical Systems* 19 (2010) 1029–1040.
- [31] W.L. Tang, D.Z. Tang, Z.H. Ni, N. Xiang, H. Yi, A portable single-cell analysis system integrating hydrodynamic trapping with broadband impedance spectroscopy, *Sci. China Technol. Sci.* 60 (2017) 1707–1715.
- [32] A.L. Alves de Araujo, J. Claudel, D. Kourtiche, M. Nadi, Influence of electrode connection tracks on biological cell measurements by impedance spectroscopy, *Sensors* 19 (2019) 2839.
- [33] S. Yan, D. Yuan, Continuous microfluidic 3D focusing enabling microflow cytometry for single-cell analysis, *Talanta* 221 (2021) 121401.
- [34] J. Chen, C. Xue, Y. Zhao, D. Chen, M.H. Wu, J. Wang, Microfluidic impedance flow cytometry enabling high-throughput single-cell electrical property characterization, *Int. J. Mol. Sci.* 16 (2015) 9804–9830.
- [35] T.A. Nguyen, T.I. Yin, D. Reyes, G.A. Urban, Microfluidic chip with integrated electrical cell-impedance sensing for monitoring single cancer cell migration in three-dimensional matrixes, *Anal. Chem.* 85 (2013) 11068–11076.
- [36] Y. Xu, X. Xie, Y. Duan, L. Wang, Z. Cheng, J. Cheng, A review of impedance measurements of whole cells, *Biosens. Bioelectron.* 77 (2016) 824–836.
- [37] F. Caselli, P. Bisegna, Simulation and performance analysis of a novel high-accuracy shearless microfluidic impedance cytometer with coplanar electrode layout, *Med. Eng. Phys.* 48 (2017) 81–89.
- [38] W. Zhao, S. Tian, L. Huang, K. Liu, L. Dong, The review of Lab-on-PCB for biomedical application, *Electrophoresis* 41 (2020) 1433–1445.
- [39] R.-J. Yang, L.-M. Fu, H.-H. Hou, Review and perspectives on microfluidic flow cytometers, *Sensor. Actuator. B Chem.* 266 (2018) 26–45.
- [40] A. Vembadi, A. Menachery, M.A. Qasaimeh, Cell cytometry: review and perspective on biotechnological advances, *Frontiers in Bioengineering and Biotechnology* 7 (2019) 147.
- [41] K. Samlali, F. Ahmadi, A.B.V. Quach, G. Soffer, S.C.C. Shih, One cell, one drop, one click: hybrid microfluidics for mammalian single cell isolation, *Small* 16 (2020), e2002400.
- [42] J. Panwar, R. Roy, Integrated Field's metal microelectrodes based microfluidic impedance cytometry for cell-in-droplet quantification, *Microelectron. Eng.* 215 (2019) 111010.
- [43] M.W. van der Helm, O.Y.F. Henry, A. Bein, T. Hamkins-Indik, M.J. Cronce, W. D. Leineweber, M. Odijk, A.D. van der Meer, J.C.T. Eijkel, D.E. Ingber, A. van den Berg, L.I. Segerink, Non-invasive sensing of transepithelial barrier function and tissue differentiation in organs-on-chips using impedance spectroscopy, *Lab Chip* 19 (2019) 452–463.
- [44] K. Senthil Kumar, P.Y. Chen, H. Ren, A Review of Printable Flexible and Stretchable Tactile Sensors, 2019, Research (Washington D C), 2019, p. 3018568.
- [45] M. Rothbauer, H. Zirath, P. Ertl, Recent advances in microfluidic technologies for cell-to-cell interaction studies, *Lab Chip* 18 (2018) 249–270.
- [46] C. Petchakup, K. Li, H. Hou, Advances in single cell impedance cytometry for biomedical applications, *Micromachines* 8 (2017) 87.
- [47] Q. Hassan, S. Ahmadi, K. Kerman, Recent advances in monitoring cell behavior using cell-based impedance spectroscopy, *Micromachines* 11 (2020) 590.
- [48] W. Tang, D. Tang, Z. Ni, N. Xiang, H. Yi, Microfluidic impedance cytometer with inertial focusing and liquid electrodes for high-throughput cell counting and discrimination, *Anal. Chem.* 89 (2017) 3154–3161.
- [49] T. Sun, H. Morgan, Single-cell microfluidic impedance cytometry: a review, *Microfluid. Nanofluidics* 8 (2010) 423–443.
- [50] H. Daguerre, M. Solsona, J. Cottet, M. Gauthier, P. Renaud, A. Bolopion, Positional dependence of particles and cells in microfluidic electrical impedance flow cytometry: origin, challenges and opportunities, *Lab Chip* 20 (2020) 3665–3689.
- [51] D. Moschou, A. Tserepi, The lab-on-PCB approach: tackling the muTAS commercial upscaling bottleneck, *Lab Chip* 17 (2017) 1388–1405.
- [52] D. Holmes, D. Pettigrew, C.H. Reccius, J.D. Gwyer, C. van Berkel, J. Holloway, D. E. Davies, H. Morgan, Leukocyte analysis and differentiation using high speed microfluidic single cell impedance cytometry, *Lab Chip* 9 (2009) 2881–2889.
- [53] H. Morgan, T. Sun, D. Holmes, S. Gawad, N.G. Green, Single cell dielectric spectroscopy, *J. Phys. Appl. Phys.* 40 (2007) 61–70.
- [54] T. Sun, S. Gawad, N.G. Green, H. Morgan, Dielectric spectroscopy of single cells: time domain analysis using Maxwell's mixture equation, *J. Phys. Appl. Phys.* 40 (2007) 1–8.
- [55] T. Sun, N.G. Green, H. Morgan, Analytical and numerical modeling methods for impedance analysis of single cells on-chip, *Nano* 3 (2008) 55–63.
- [56] K. Asami, Characterization of heterogeneous systems by dielectric spectroscopy, *Prog. Polym. Sci.* 27 (2002) 1617–1659.
- [57] K. Asami, Dielectric dispersion in biological cells of complex geometry simulated by the three-dimensional finite difference method, *J. Phys. Appl. Phys.* 39 (2006) 492–499.
- [58] H.G. Chun, T.D. Chung, H.C. Kim, Cytometry and velocimetry on a microfluidic chip using polyelectrolytic salt bridges, *Anal. Chem.* 77 (2005) 2490–2495.
- [59] J. Chen, Y. Zheng, Q.Y. Tan, E. Shojaei-Baghini, Y.L. Zhang, J. Li, P. Prasad, L. D. You, X.Y. Wu, Y. Sun, Classification of cell types using a microfluidic device for mechanical and electrical measurement on single cells, *Lab Chip* 11 (2011) 3174–3181.
- [60] Y. Zhang, Y. Zhao, D. Chen, K. Wang, Y. Wei, Y. Xu, C. Huang, J. Wang, J. Chen, Crossing constriction channel-based microfluidic cytometry capable of electrically phenotyping large populations of single cells, *Analyst* 144 (2019) 1008–1015.
- [61] K.R. Foster, H.P. Schwan, Dielectric-properties of tissues and biological-materials - a critical-review, *Crit. Rev. Biomed. Eng.* 17 (1989) 25–104.
- [62] S.M.A. Iqbal, N.Z. Butt, Design and analysis of microfluidic cell counter using spice simulation, *SN Applied Sciences* 1 (2019) 1–10.
- [63] T. Sun, H. Morgan, N.G. Green, Analytical solutions of ac electrokinetics in interdigitated electrode arrays: electric field, dielectrophoretic and traveling-wave dielectrophoretic forces, *Phys. Rev.* 76 (2007) 46610.
- [64] I. Heidmann, G. Schade-Kampmann, J. Lambalk, M. Ottiger, M. Di Berardino, Impedance flow cytometry: a novel technique in pollen analysis, *PloS One* 11 (2016), e0165531.
- [65] Z. Lin, S.Y. Lin, P. Xie, C.Y. Lin, G.M. Rather, J.R. Bertino, M. Javanmard, Rapid assessment of surface markers on cancer cells using immuno-magnetic separation and multi-frequency impedance cytometry for targeted therapy, *Sci. Rep.* 10 (2020) 3015.
- [66] P.A. Duarte, L. Menze, G.N. Abdelrasoul, S. Yosinski, Z. Kobos, R. Stuermer, M. Reed, J. Yang, X.S. Li, J. Chen, Single ascospore detection for the forecasting of *Sclerotinia* stem rot of canola, *Lab Chip* 20 (2020) 3644–3652.
- [67] C.H. Ren, S.H. Zhang, D. Song, J.H. Guo, Lab on dielectric film deposited PCB device for characterization of electrical property of biological cells, *IEEE Trans. Dielectr. Electr. Insul.* 23 (2016) 1895–1897.
- [68] J. Sui, P. Xie, Z. Lin, M. Javanmard, Electronic classification of barcoded particles for multiplexed detection using supervised machine learning analysis, *Talanta* 215 (2020) 120791.
- [69] J. Cottet, A. Kehren, H. van Lintel, F. Buret, M. Fréne-Robin, P. Renaud, How to improve the sensitivity of coplanar electrodes and micro channel design in

- electrical impedance flow cytometry: a study, *Microfluid. Nanofluidics* 23 (2019) 1–11.
- [70] D.C. Rees, T.N. Williams, M.T. Gladwin, Sickle-cell disease, *Lancet* 376 (2010) 2018–2031.
- [71] X. Xie, Z. Zhang, X. Ge, X. Zhao, L. Hao, Z. Cheng, W. Zhou, Y. Du, L. Wang, F. Tian, X. Xu, Particle self-aligning, focusing, and electric impedance microcytometer device for label-free single cell morphology discrimination and yeast budding analysis, *Anal. Chem.* 91 (2019) 13398–13406.
- [72] Z. Zhu, W. Chen, B. Tian, Y. Luo, J. Lan, D. Wu, D. Chen, Z. Wang, D. Pan, Using microfluidic impedance cytometry to measure *C. elegans* worms and identify their developmental stages, *Sensor. Actuator. B Chem.* 275 (2018) 470–482.
- [73] B. Brazej, J. Cottet, A. Bolopion, H. Van Lintel, P. Renaud, M. Gauthier, Impedance-based real-time position sensor for lab-on-a-chip devices, *Lab Chip* 18 (2018) 818–831.
- [74] H. Wang, N. Sobahi, A. Han, Impedance spectroscopy-based cell/particle position detection in microfluidic systems, *Lab Chip* 17 (2017) 1264–1269.
- [75] Q. Zi, W. Ding, C. Sun, S. Li, D. Gao, L. He, J. Liu, L. Xu, B. Qiu, On-chip label-free determination of cell survival rate, *Biosens. Bioelectron.* 148 (2020) 111820.
- [76] Y. Feng, L. Huang, P. Zhao, F. Liang, W. Wang, A microfluidic device integrating impedance flow cytometry and electric impedance spectroscopy for high-efficiency single-cell electrical property measurement, *Anal. Chem.* 91 (2019) 15204–15212.
- [77] S. Gawad, L. Schild, P.H. Renaud, Micromachined impedance spectroscopy flow cytometer for cell analysis and particle sizing, *Lab Chip* 1 (2001) 76–82.
- [78] S.P. Desai, A. Coston, A. Berlin, Micro-electrical impedance spectroscopy and identification of patient-derived, dissociated tumor cells, *IEEE Trans. NanoBioscience* 18 (2019) 369–372.
- [79] A. De Ninno, R. Reale, A. Giovinazzo, F.R. Bertani, L. Businaro, P. Bisegna, C. Matteucci, F. Caselli, High-throughput label-free characterization of viable, necrotic and apoptotic human lymphoma cells in a coplanar-electrode microfluidic impedance chip, *Biosens. Bioelectron.* 150 (2020) 111887.
- [80] C. Petchakup, H.M. Tay, W.H. Yeap, R. Dalan, S.C. Wong, K.H.H. Li, H.W. Hou, Label-free leukocyte sorting and impedance-based profiling for diabetes testing, *Biosens. Bioelectron.* 118 (2018) 195–203.
- [81] C. Petchakup, H.M. Tay, K.H.H. Li, H.W. Hou, Integrated inertial-impedance cytometry for rapid label-free leukocyte isolation and profiling of neutrophil extracellular traps (NETs), *Lab Chip* 19 (2019) 1736–1746.
- [82] C. Petchakup, P.E. Hutchinson, H.M. Tay, S.Y. Leong, K.H.H. Li, H.W. Hou, Label-free quantitative lymphocyte activation profiling using microfluidic impedance cytometry, *Sensor. Actuator. B Chem.* 339 (2021) 129864.
- [83] J. Claudel, A.L. Alves De Araujo, M. Nadi, D. Kourtiche, Lab-on-A-chip device for yeast cell characterization in low-conductivity media combining cytometry and bio-impedance, *Sensors* 19 (2019) 3366.
- [84] K. Mahesh, M. Varma, P. Sen, Double-peak signal features in microfluidic impedance flow cytometry enable sensitive measurement of cell membrane capacitance, *Lab Chip* 20 (2020) 4296–4309.
- [85] L.Y. Gong, C. Petchakup, P.J. Shi, P.L. Tan, L.P. Tan, C.Y. Tay, H.W. Hou, Direct and label-free cell status monitoring of spheroids and microcarriers using microfluidic impedance cytometry, *Small* (2021), e2007500.
- [86] D. Tang, M. Chen, Y. Han, N. Xiang, Z. Ni, Asymmetric serpentine microchannel based impedance cytometer enabling consistent transit and accurate characterization of tumor cells and blood cells, *Sensor. Actuator. B Chem.* 336 (2021) 129719.
- [87] M. Serhatlioglu, M. Asghari, M.T. Guler, C. Elbukten, Impedance-based viscoelastic flow cytometry, *Electrophoresis* 40 (2019) 906–913.
- [88] A. De Ninno, V. Errico, F.R. Bertani, L. Businaro, P. Bisegna, F. Caselli, Coplanar electrode microfluidic chip enabling accurate sheathless impedance cytometry, *Lab Chip* 17 (2017) 1158–1166.
- [89] F. Caselli, A. De Ninno, R. Reale, L. Businaro, P. Bisegna, A Bayesian approach for coincidence resolution in microfluidic impedance cytometry, *IEEE Trans. Biomed. Eng.* 68 (2020) 340–349.
- [90] F. Caselli, M. Shaker, L. Colella, P. Renaud, P. Bisegna, Modeling, simulation, and performance evaluation of a novel microfluidic impedance cytometer for morphology-based cell discrimination, *Journal of Microelectromechanical Systems* 23 (2014) 785–794.
- [91] M. Shaker, L. Colella, F. Caselli, P. Bisegna, P. Renaud, An impedance-based flow microcytometer for single cell morphology discrimination, *Lab Chip* 14 (2014) 2548–2555.
- [92] D. Yang, Y. Ai, Microfluidic impedance cytometry device with N-shaped electrodes for lateral position measurement of single cells/particles, *Lab Chip* 19 (2019) 3609–3617.
- [93] R. Reale, A. De Ninno, L. Businaro, P. Bisegna, F. Caselli, High-throughput electrical position detection of single flowing particles/cells with non-spherical shape, *Lab Chip* 19 (2019) 1818–1827.
- [94] Z. Han, L. Chen, S. Zhang, J. Wang, X. Duan, Label-free and simultaneous mechanical and electrical characterization of single plant cells using microfluidic impedance flow cytometry, *Anal. Chem.* 92 (2020) 14568–14575.
- [95] Y. Zhou, D. Yang, Y. Zhou, B.L. Khoo, J. Han, Y. Ai, Characterizing deformability and electrical impedance of cancer cells in a microfluidic device, *Anal. Chem.* 90 (2018) 912–919.
- [96] S. Afshar, E. Salimi, A. Fazelkhan, K. Braasch, N. Mishra, M. Butler, D.J. Thomson, G.E. Bridges, Progression of change in membrane capacitance and cytoplasm conductivity of cells during controlled starvation using dual-frequency DEP cytometry, *Anal. Chim. Acta* 1059 (2019) 59–67.
- [97] N. Wang, R. Liu, N. Asmare, C.H. Chu, A.F. Sarioglu, Processing code-multiplexed Coulter signals via deep convolutional neural networks, *Lab Chip* 19 (2019) 3292–3304.
- [98] N.Q. Wang, R.X. Liu, N. Asmare, C.H. Chu, A.F. Sarioglu, Integrated sensor networks with error correction for multiplexed particle tracking in microfluidic chips, *Biosens. Bioelectron.* 174 (2021) 112818.
- [99] S. Gawad, T. Sun, N.G. Green, H. Morgan, Impedance spectroscopy using maximum length sequences: application to single cell analysis, *Rev. Sci. Instrum.* 78 (2007) 54301.
- [100] N. Haandbaek, O. With, S.C. Burgel, F. Heer, A. Hierlemann, Resonance-enhanced microfluidic impedance cytometer for detection of single bacteria, *Lab Chip* 14 (2014) 3313–3324.
- [101] X.D. Wu, Y.J. Kang, Y.N. Wang, D.Y. Xu, D.Y. Li, D.Q. Li, Microfluidic differential resistive pulse sensors, *Electrophoresis* 29 (2008) 2754–2759.
- [102] T. Sun, D. Holmes, S. Gawad, N.G. Green, H. Morgan, High speed multi-frequency impedance analysis of single particles in a microfluidic cytometer using maximum length sequences, *Lab Chip* 7 (2007) 1034–1040.
- [103] S. Gawad, K. Cheung, U. Seger, A. Bertsch, P. Renaud, Dielectric spectroscopy in a micromachined flow cytometer: theoretical and practical considerations, *Lab Chip* 4 (2004) 241–251.
- [104] D. Spencer, V. Hollis, H. Morgan, Microfluidic impedance cytometry of tumour cells in blood, *Biomicrofluidics* 8 (2014), 064124.
- [105] J.S. McGrath, C. Honrado, D. Spencer, B. Horton, H.L. Bridle, H. Morgan, Analysis of parasitic Protozoa at the single-cell level using microfluidic impedance cytometry, *Sci. Rep.* 7 (2017) 2601.
- [106] C. Honrado, N. Michel, J.H. Moore, A. Salahi, V. Porterfield, M.J. McConnell, N. S. Swami, Label-free quantification of cell cycle synchronicity of human neural progenitor cells based on electrophysiology phenotypes, *ACS Sens.* 6 (2021) 156–165.
- [107] C.H. Clausen, M. Dimaki, C.V. Bertelsen, G.E. Skands, R. Rodriguez-Trujillo, J. D. Thomsen, W.E. Svendsen, Bacteria detection and differentiation using impedance flow cytometry, *Sensors* 18 (2018) 3496.
- [108] J.H. Moore, A. Salahi, C. Honrado, C. Warburton, C.A. Warren, N.S. Swami, Quantifying bacterial spore germination by single-cell impedance cytometry for assessment of host microbiota susceptibility to Clostridioides difficile infection, *Biosens. Bioelectron.* 166 (2020) 112440.
- [109] S.I. Han, K.H. Han, Electrical detection method for circulating tumor cells using graphene nanoplates, *Anal. Chem.* 87 (2015) 10585–10592.
- [110] N. Haandbaek, S.C. Burgel, F. Rudolf, F. Heer, A. Hierlemann, Characterization of single yeast cell phenotypes using microfluidic impedance cytometry and optical imaging, *ACS Sens.* 1 (2016) 1020–1027.
- [111] F. Caselli, R. Reale, N.A. Nodargi, P. Bisegna, Numerical investigation of a NovelWiring scheme enabling simple and accurate impedance cytometry, *Micromachines* 8 (2017) 283.
- [112] D. Spencer, H. Morgan, Positional dependence of particles in microfluidic impedance cytometry, *Lab Chip* 11 (2011) 1234–1239.
- [113] D. Spencer, F. Caselli, P. Bisegna, H. Morgan, High accuracy particle analysis using sheathless microfluidic impedance cytometry, *Lab Chip* 16 (2016) 2467–2473.
- [114] D. Spencer, H. Morgan, High-speed single-cell dielectric spectroscopy, *ACS Sens.* 5 (2020) 423–430.
- [115] J.S. McGrath, C. Honrado, J.H. Moore, S.J. Adair, W.B. Varhue, A. Salahi, V. Farmehini, B.J. Goudreau, S. Nagdas, E.M. Blais, T.W. Bauer, N.S. Swami, Electrophysiology-based stratification of pancreatic tumorigenicity by label-free single-cell impedance cytometry, *Anal. Chim. Acta* 1101 (2020) 90–98.
- [116] F. Caselli, A. De Ninno, R. Reale, L. Businaro, P. Bisegna, A novel wiring scheme for standard chips enabling high-accuracy impedance cytometry, *Sensor. Actuator. B Chem.* 256 (2018) 580–589.
- [117] D.C. Spencer, T.F. Paton, K.T. Mulroney, T.J.J. Inglis, J.M. Sutton, H. Morgan, A fast impedance-based antimicrobial susceptibility test, *Nat. Commun.* 11 (2020) 5328.
- [118] D.H. Yang, Y. Zhou, Y.N. Zhou, J. Han, Y. Ai, Biophysical phenotyping of single cells using a differential multiconstriction microfluidic device with self-aligned 3D electrodes, *Biosens. Bioelectron.* 133 (2019) 16–23.
- [119] M. Mansor, M. Takeuchi, M. Nakajima, Y. Hasegawa, M. Ahmad, Electrical impedance spectroscopy for detection of cells in suspensions using microfluidic device with integrated microneedles, *Appl. Sci.* 7 (2017) 170.
- [120] E. Rollo, E. Tenaglia, R. Genolet, E. Bianchi, A. Harari, G. Coukos, C. Guiducci, Label-free identification of activated T lymphocytes through tridimensional microsensors on chip, *Biosens. Bioelectron.* 94 (2017) 193–199.
- [121] M. Solsona, E.Y. Westerbeek, J.G. Bomer, W. Olthuis, A. van den Berg, Gradient in the electric field for particle position detection in microfluidic channels, *Lab Chip* 19 (2019) 1054–1059.
- [122] R.W. Deblois, C.P. Bean, Counting and sizing of submicron particles by resistive pulse technique, *Rev. Sci. Instrum.* 41 (1970) 909–916.
- [123] M.L. Shuler, H.M. Tsuchiya, R. Aris, Hydrodynamic focusing and electronic cell-sizing techniques, *Appl. Microbiol.* 24 (1972) 384–388.
- [124] R.A. Hoffman, W.B. Britt, Flow-system measurement of cell impedance properties, *J. Histochem. Cytochem.* 27 (1979) 234–240.
- [125] R.A. Hoffman, T.S. Johnson, W.B. Britt, Flow cytometric electronic direct-current volume and radiofrequency impedance measurements of single cells and particles, *Cytometry* 1 (1981) 377–384.
- [126] T.-K. Chiu, Y. Zhao, D. Chen, C.-H. Hsieh, K. Wang, W.-P. Chou, C.-J. Liao, H.-Y. Wang, B. Fan, J. Wang, J. Chen, M.-H. Wu, A low-sample-loss microfluidic system for the quantification of size-independent cellular electrical property—its

- demonstration for the identification and characterization of circulating tumour cells (CTCs), *Sensor. Actuator. B Chem.* 246 (2017) 29–37.
- [127] W. Zhang, Y. Hu, G. Choi, S. Liang, M. Liu, W. Guan, Microfluidic multiple cross-correlated Coulter counter for improved particle size analysis, *Sensor. Actuator. B Chem.* 296 (2019) 126615.
- [128] G. Choi, E. Murphy, W. Guan, Microfluidic time-division multiplexing accessing resistive pulse sensor for particle analysis, *ACS Sens.* 4 (2019) 1957–1963.
- [129] A. Valero, T. Braschler, P. Renaud, A unified approach to dielectric single cell analysis: impedance and dielectrophoretic force spectroscopy, *Lab Chip* 10 (2010) 2216–2225.
- [130] Z. Mei, Z. Liu, Z. Zhou, A compact and low cost microfluidic cell impedance detection system, *AIMS Biophysics* 3 (2016) 596–608.
- [131] G. Mernier, E. Duqi, P. Renaud, Characterization of a novel impedance cytometer design and its integration with lateral focusing by dielectrophoresis, *Lab Chip* 12 (2012) 4344–4349.
- [132] A.V. Jagtiani, J. Carletta, J. Zhe, A microfluidic multichannel resistive pulse sensor using frequency division multiplexing for high throughput counting of micro particles, *J. Micromech. Microeng.* 21 (2011), 065004.